Oral Presentation

170 Structural and metabolic dynamics of plant cells in context of heat acclimation
Charlotte Seydel[1,3], Prof. Dr. Martin Heß[2], Prof. Dr. Thomas Nägele[3], Prof. Dr. Andreas Klingl[1]
[1]Ludwig-Maximilians-Universität München, Faculty of Biology, Plant Development, Planegg-Martinsried, Germany, [2]Ludwig-Maximilians-Universität München, Faculty of Biology, Systematic Zoology, Planegg-Martinsried, Germany, [3]Ludwig-Maximilians-Universität München, Faculty of Biology, Plant Evolutionary Cell Biology, Planegg-Martinsried, Germany
430 Exploring the infection cycle of Vaccinia virus using 3D EM with the FIB-SEM
Sandra Sara[1]
[1]Université Paris-Saclay, CEA, CNRS, Institute for Integrative Biology of the Cell (I2BC), Gif-Sur-Yvette, France
436 Three-dimensional imaging to study early bone mineralization
Dr Elena Macías-Sánchez[1], Dr Emeline Raguin[2], Dr Nadezda Tarakina[3], Prof Peter Fratzl[2]
[1]Department of Stratigraphy and Paleontology, University of Granada, Granada, Spain, [2]Department of Biomaterials, Max Planck Institute of Colloids and Interfaces, Potsdam, Germany, [3]Department of Colloid Chemistry, Max Planck Institute of Colloids and Interfaces, Potsdam, Germany
493 The ultrastructural analysis of plant-microbe interfaces
Isabella Gantner[1], Dr. Julia Buchner[1], Prof. Dr. Andreas Klingl[1]
[1]Plant Development and Electron microscopy, Ludwig-Maximilians-Universität, Munich, Germany
677 FIB-SEM and automatic segmentation for investigation of mitochondrial organization in cells of urinary bladder urothelium
Samo Hudoklin[1], Bruno Humbel[2], Manca Žerovnik Mekuč[3], Ciril Bohak[3], Matija Marolt[3], Rok Romih[1]
[1]Institute of Cell Biology, Faculty of Medicine, University of Ljubljana, Ljubljana, Slovenia, [2]Electron Microscopy Facility, University of Lausanne , Lausanne, Swizerland, [3]Faculty of Computer and Information Science, University of Ljubljana, Ljubljana, Slovenia
850 3D TEM and SEM-array tomography of Hailey-Hailey Disease human skin biopsies
Ph.D. Massimo Micaroni[1], P.D. Jens Berndtsson[1], P.D. Rafael Camacho[1], Ph.D. Erin Cocks[1], M.D. Giulio Gualdi[2], Ph.D. Apollonia Tullo[3], Ph.D. Flaviana Marzano[3], M.D. Camilla Marinelli[4], Ph.D. Anna Campanati[5], M.D. Gaetana Lanzi[6], M.D., Ph.D. Manuela Iezzi[7], M.D. Vincenzo Maione[8], M.D., Ph.D. Paolo Amerio[2], Ph.D. Julia Fernandez-Rodriguez[1]
[1]Centre for Cellular Imaging Core Facility, Sahlgrenska Academy, University of Gothenburg, Göteborg, Sweden, [2]Department of Medicine and Aging Science, Dermatology Unit, University “G. d'Annunzio”, Chieti-Pescara, Italy, [3]Institute of Biomembranes, Bioenergetic and Molecular Biotechnology – IBIOM, Bari, Italy, [4]UOSD Pathological Anatomy, ASL 2 Abruzzo, “G. Bernabeo” Hospital, Ortona (CH), Italy, [5]Department of Clinical and Molecular Sciences, Dermatology Clinic, Polytechnic Marche University, Ancona, Italy, [6]Medical Genetics Laboratory, Diagnostic Department, ASST-Spedali Civili of Brescia, Brescia, Italy, [7]Department of Neuroscience, Imaging and Clinical Sciences, Pathology Section, University “G. d'Annunzio” Chieti-Pescara, Chieti-Pescara, Italy, [8]Dermatology, ASST-Spedali Civili of Brescia, Brescia, Italy
942 Differential axon terminal spread and synapse numbers amongst afferent neurons onto a locust's movement detector
Assoc. Prof. Dr Gerd Leitinger[1], Snjezana Radulovic[1], Dr Erin Cocks[3], Dr Claire Rind[3]
[1]Division of Cell Biology, Histology and Embryology, Gottfried Schatz Research Center, Medical University of Graz, Graz, Austria, [2]Electron Microscopy Research Services, Faculty of Medical Sciences, Newcastle University, Newcastle upon Tyne, UK, [3]Biosciences Institute, Faculty of Medical Sciences, Newcastle University, , Newcastle upon Tyne, UK
1244 Volume Electron Microscopy: A Powerful Tool for Studying Embryonic Pineal Organ Development in Birds
Prof. Bogdan Lewczuk[1], Dr Natalia Szyrynska[1], Dr Magdalena Prusik[1]

[1]University Of Warmia And Mazury In Olsztyn, Olsztyn, Poland

Poster Presentation

81 How Euro-BioImaging can support your research with access to the best imaging tools
Johanna Bischof[1]
[1]Euro-BioImaging ERIC, Heidelberg, Germany
832 Exit of different cargoes from the Golgi and their post-Golgi trafficking
Dr. Galina Beznoussenko[1], PhD, MD, Prof. Alexander Mironov[1]
[1]IFOM ETS, The AIRC Institute of Molecular Oncology, Via Adamello 16, 20139, Milan, Italy, Milan, Italy
835 Investigating Bone Microstructure with ATUM-SEM: Implications for Pathological Conditions
Ph.d Valeria Vistoso[1], Dr. Tom Fertè[1], Dr. Federica Buccino[2], Professor Laura Maria Vergani[2], Professor Ovidiu Ersen[1], Professor Adele Carradò[1]
[1]Institut de physique et chimie des Matériaux de Strasbourg, University of Strasbourg, Strasbourg, France, [2]Department of Mechanical Engineering, Politecnico di Milano, Milan, Italy
876 Ultrastructural analysis of liver injury and regeneration after microcystin-LR intoxication in whitefish
PhD Natalia Szyrynska[1], Bogdan Lewczuk[1], Maciej Wozny[2], Pawel Brzuzan[2]
[1]Department of Histology and Embryology, Faculty of Veterinary Medicine, University of Warmia and Mazury in Olsztyn , , Poland, [2]Department of Environmental Biotechnology, Faculty of Geoengineering, University of Warmia and Mazury in Olsztyn, , Poland
891 Three-dimensional ultrastructure of ovine pinealocytes
Prof. Bogdan Lewczuk[1], Dr Natalia Szyrynska[1]
[1]Department of Histology and Embryology, Faculty of Veterinary Medicine, University of Warmia and Mazury in Olsztyn, , Poland
917 Simple and efficient three-dimensional reconstruction method of plant cells using transmission electron microscope
Ms. Haruka Aoki[1], Ms. Mizuki Matsuzaki[1], Mr. Hideo Nishioka[1], Ms. Chieko Hamamoto[1]
[1]JEOL Ltd., Akishima, Japan
956 Sample preparation for correlative light, soft X-ray tomography, and cryo FIB-SEM imaging of biological cells
Director Imaging Applications Sergey Kapishnikov[1], Maryna Kobylynska[2,3], Prof. Roland A. Fleck[2,3], Malene Fog Lihme Olsen[4], Prof. Poul Erik Jensen[4], Dr Kenneth Fahy[1], Dr Paul Sheridan[1], Dr William Fyans[1], Dr Fergal O'Reilly[1,5,6], Tony McEnroe[1]
[1]SiriusXT Ltd., Dublin, Ireland, [2]Randall Centre for Cell and Molecular Biophysics, King's College London, London, United Kingdom, [3]Centre for Ultrastructural Imaging, King's College London, London, United Kingdom, [4]Department of Food Science, University of Copenhagen, Copenhagen, Denmark, [5]School of Physics, University College Dublin, Dublin, Ireland, [6]School of Biology and Environmental Sciences, University College Dublin, Dublin, Ireland
1125 Depositing biological segmentation datasets FAIRly
Dr Elaine Ho[1], Dr Dimitris Ladakis[1], Dr Michele C. Darrow[1]
[1]Artificial Intelligence and Informatics, The Rosalind Franklin Institute, Harwell, United Kingdom

Late Poster Presentation

1174 The Impact of Dietary Haemoglobin on Nymphal Stages of I.ricinus: The gut volume EM reconstruction
Mgr., M.sc. František Kitzberger[1,2], RNDr. Ph.D. Veronika Urbanová[1], RNDr. CSc. Petr Kopáček[1], RNDr. Ph.D. Daniel Sojka[1], Mgr. Ph.D. Jan Perner[1], RNDr. Ph.D. Marie Vancová[1]

[1]Institute of Parasitology, Biology Centre of the Czech Academy of Sciences, Ceske Budejovice, Czech Republic, [2]Faculty of Science, Department of Physics, University of South Bohemia, Ceske Budejovice, Czech Republic

1230 Tracking the Ultrastructure of Life with Serial Block-face Scanning Electron Microscopy

Dr. Alexandra Elli[1], Dr. Nathalie Braun[2], Dr. Dieter Lauer[2]

[1]Carl Zeiss Microscopy GmbH, Jena, Germany, [2]Carl Zeiss Microscopy GmbH, Oberkochen, Germany

1239 3D imaging by Array Tomography using benchtop SEM

Kaori Nakajima[1], Yuuki Yamaguchi[1], Daisuke Masuda[1], Junichi Nakakobaru[2], Motohiro Nakamura[1], Katsuyuki Suzuki[1], Yukari Moriya[1], Yasuyuki Okano[1]

[1]JEOL Ltd., Akishima, JAPAN, [2]SYSTEM IN FRONTIER INC., Tachikawa, JAPAN

1279 3D chromatin architecture by volume EM

Dr. Dusan Cmarko[1], Dr. Pavla Molinova[1], M.Sc. Marketa Dalecka[2], Dr. Ales Benda[3]

[1]Institute of Biology and Medical Genetics, First Faculty of Medicine, Charles University and General University Hospital in Prague, Prague, Czech Republic, [2]Imaging Methods Core Facility at BIOCEV and Department of Genetics and Microbiology, Faculty of Science, Charles University, Prague, Czech Republic, [3]Imaging Methods Core Facility at BIOCEV, Faculty of Science, Charles University, Prague, Czech Republic

170

Structural and metabolic dynamics of plant cells in context of heat acclimation

Charlotte Seydel[1,3], Prof. Dr. Martin Heß[2], Prof. Dr. Thomas Nägele[3], Prof. Dr. Andreas Klingl[1]
[1]Ludwig-Maximilians-Universität München, Faculty of Biology, Plant Development, Planegg-Martinsried, Germany, [2]Ludwig-Maximilians-Universität München, Faculty of Biology, Systematic Zoology, Planegg-Martinsried, Germany, [3]Ludwig-Maximilians-Universität München, Faculty of Biology, Plant Evolutionary Cell Biology, Planegg-Martinsried, Germany

LS-07 (1), Lecture Theater 4, august 28, 2024, 11:30 - 12:30

Background incl. aims
In order to survive sub-lethal heat stress, plants possess the ability to acclimate to moderately elevated temperature. They are altering their physiology in many different ways to maintain cellular homeostasis despite the change in environmental conditions. The carbohydrate metabolism is important for energy storage and biomass production and is also involved in regulation of heat acclimation response. To accurately resolve subcellular metabolic fluxes and compartment specific metabolite concentrations in the model organism Arabidopsis thaliana, it is necessary to combine ultrastructural and metabolic data.
Methods
A non-aqueous fractionation procedure to determine subcellular metabolite concentrations was combined with 3D imaging of leaf tissue by serial block-face scanning electron microscopy, which resulted in two datasets of control and heat treated samples.
Results
We were able to generate a dataset of subcellular volumes of A. thaliana leaf tissue. This allowed us to calculate effective metabolite concentrations in three compartments of the cell, namely cytosol, vacuole and chloroplasts. Applying a kinetic model of carbohydrate metabolism, subcellular fluxes were estimated which revealed metabolic heat acclimation strategies of plant metabolism and provide evidence for a tightly regulated metabolic network.
Conclusion
The combination of microscopic techniques with metabolic and photosynthetic measurements allows a more holistic interpretation of plant heat acclimation and can help preventing misinterpretation of the individual datasets.

Keywords:

heat acclimation arabidopsis carbohydrates SBF-SEM

Reference:

Denk, W., & Horstmann, H. (2004). Serial block-face scanning electron microscopy to reconstruct three-dimensional tissue nanostructure. PLoS Biol.
Fürtauer, L., Weckwerth, W., & Nägele, T. (2016). A benchtop fractionation procedure for subcellular analysis of the plant metabolome. Front Plant Sci.
Seydel, C., Kitashova, A., Fürtauer, L., & Nägele, T. (2022). Temperature-induced dynamics of plant carbohydrate metabolism. Physiol. Plant.

430

Exploring the infection cycle of Vaccinia virus using 3D EM with the FIB-SEM

Sandra Sara[1]
[1]Université Paris-Saclay, CEA, CNRS, Institute for Integrative Biology of the Cell (I2BC), Gif-Sur-Yvette, France

LS-07 (1), Lecture Theater 4, august 28, 2024, 11:30 - 12:30

Background incl. aims
Since its successful use as a live vaccine to eradicate Variola virus, the etiologic agent of smallpox, Vaccinia virus (VACV) has become a model to study the mechanisms underlying key processes of infection by poxviruses. At early stages of infection, viral genome replication takes place in the replication compartments, also known as viral factories. Following early viral genome replication, these viral factories subsequently seem to dissociate concomitant with VACV assembly that rely on a unique membrane acquisition mechanism. In brief, assembly of new virions involves the recruitment of vesicles from the endoplasmic reticulum, which are then ruptured-open and associate as crescents with open membrane ends. After packaging of the viral genome, the crescents are closed, forming the spherical immature virions. We aim to decipher the remodeling of VACV-infected cells during the stages of virion assembly by 3D reconstruction using the FIB-SEM technology.

Methods
Cells are cultured and infected with VACV Western Reserve strain on glass coverslips, followed by fixation using aldehyde. Subsequent steps involve post-fixation and staining with osmium tetroxide and uranyl acetate. After dehydration with an ethanol gradient, the cells are embedded in araldite resin and polymerized for 48 hours at 60°C. The resin blocks are then mounted on the FIB-SEM stub using argent lacquer, with cells protected by a platinum layer. To acquire a 3D volume, the slice-and-view approach is employed, starting with acquisition of an image stack. Subsequently, the raw images are pre-aligned using the SIFT algorithm through translation to create a template. Then, the raw data is aligned with the template created using affine transformations. Once the volume is obtained, segmentation can be performed using various software tools for subsequent data analysis.

Results
Spatial reorganization of VACV-infected HeLa cells was investigated through the acquisition of slices from a 3D volume at 8 hours post-infection, employing a FIB-SEM Cross-beam 550 system. The images, captured using electrons backscattered by the EsB detector, exhibited a pixel resolution and slice thickness of 15 nm each. Within the acquired volume, discernible changes in the organization of the endoplasmic reticulum (ER) were observed, indicative of the VACV viral replication compartment. Additionally, crescent-shaped membranes were evident in the assembly compartment, suggesting ongoing viral assembly processes. . These findings are presented in 3D format following segmentation of the various compartments and VACV virions.

Conclusion
We successfully optimized the sample preparation protocols for 3D EM analysis by FIB-SEM of VACV-infected HeLa cells. Additionally, we established an imaging workflow and implemented data acquisition of large volumes using the FIB-SEM slice and view approach. Through these efforts, we elucidated the virus-induced cellular reorganization, revealing the presence of the viral replication compartment, along with assembly involving both immature and mature virions.

Keywords:

FIB-SEM, Vaccinia Virus, ER Segmentation

Reference:

Kizilyaprak, Caroline, Anne Greet Bittermann, et al. « FIB-SEM Tomography in Biology ». Electron Microscopy, édité par John Kuo, vol. 1117, Humana Press, 2014, p. 541-58.
Carina Bahn, « Characterization of the cellular organization during Vaccina virus replication and assembly by fluorescence microscopy », a thesis submitted in fulfilment of the requirements for the degree of Master of Science at Medical School Hannover.
Hennies, J., Lleti, J.M.S., Schieber, N.L. et al. AMST: Alignment to Median Smoothed Template for Focused Ion Beam Scanning Electron Microscopy Image Stacks. Sci Rep 10, 2004 (2020).

436

Three-dimensional imaging to study early bone mineralization

Dr Elena Macías-Sánchez[1], Dr Emeline Raguin[2], Dr Nadezda Tarakina[3], Prof Peter Fratzl[2]
[1]Department of Stratigraphy and Paleontology, University of Granada, Granada, Spain, [2]Department of Biomaterials, Max Planck Institute of Colloids and Interfaces, Potsdam, Germany, [3]Department of Colloid Chemistry, Max Planck Institute of Colloids and Interfaces, Potsdam, Germany

LS-07 (2), Lecture Theater 5, august 28, 2024, 14:00 - 16:00

Background incl. aims
Two-dimensional imaging represents a serious limitation when studying the structure of complex hierarchical materials such as bone. Three-dimensional visualization is essential for understanding the interactions that occur between the cellular network, collagen fibrils, and mineral precursors during the formation process. Over the last decade, FIB-SEM has revolutionized the study of mineralized tissues, providing not only three dimensional information in the nanometer range, but also the possibility to nanofabricate mineralized lamellae avoiding the mechanical stress caused by standard sectioning techniques.
These technical advances helped elucidate the mineral deposition in collagen-based materials, driven by a spherulitic-like crystal growth [1]. Initially, disordered mineral aggregates form in the interfibrillar spaces, and subsequently the mineral infiltrates adjacent collagen fibrils, which provide the structural framework for the formation of layered spherulites. These spherulites (also called mineral ellipsoids) imbricate forming a new hierarchical level of organization in bone termed tessellation [2]. Although the mechanism has been described in several systems [1, 2, 3], detailed data on the interaction of the organic and the mineral phases remain insufficient.
Methods
The present study combines electron tomography (FIB-SEM serial surface imaging) which provides 3D information, with the fabrication of lamellae for scanning/transmission electron microscopy (S/TEM), selected area electron diffraction (SAED) and energy dispersive spectroscopy (EDS) chemical mapping to elucidate crystal distribution and orientation throughout the collagen matrix.
Results
The study reveals the internal structure of the forming fibrolamellar bone at nanometer resolution. A connective tissue with dispersed and non-preferentially oriented collagen fibrils seems to be deposited first, serving as a scaffold for the deposition of more aligned collagen. During embryonic development, these osteocytes initiate the mineralization process and become buried in the mineral matrix, which expands both vertically and laterally to form the nascent fibrolamellar units. At the collagen-mineral interface, a multitude of mineral spherulites proliferate and grow to confluence. Their profiles are still recognizable in the consolidated mineral layer.
Conclusions
Our study confirms that the formation of mineral spherulites also drives the mineral deposition in embryonic fibrolamellar bone. This fact demonstrates that this protein-mediated crystal growth mechanism occurs in different types of bone tissue and in different species, indicating that it is a common and homologous mineralization mechanism in type I collagen-based materials [4].

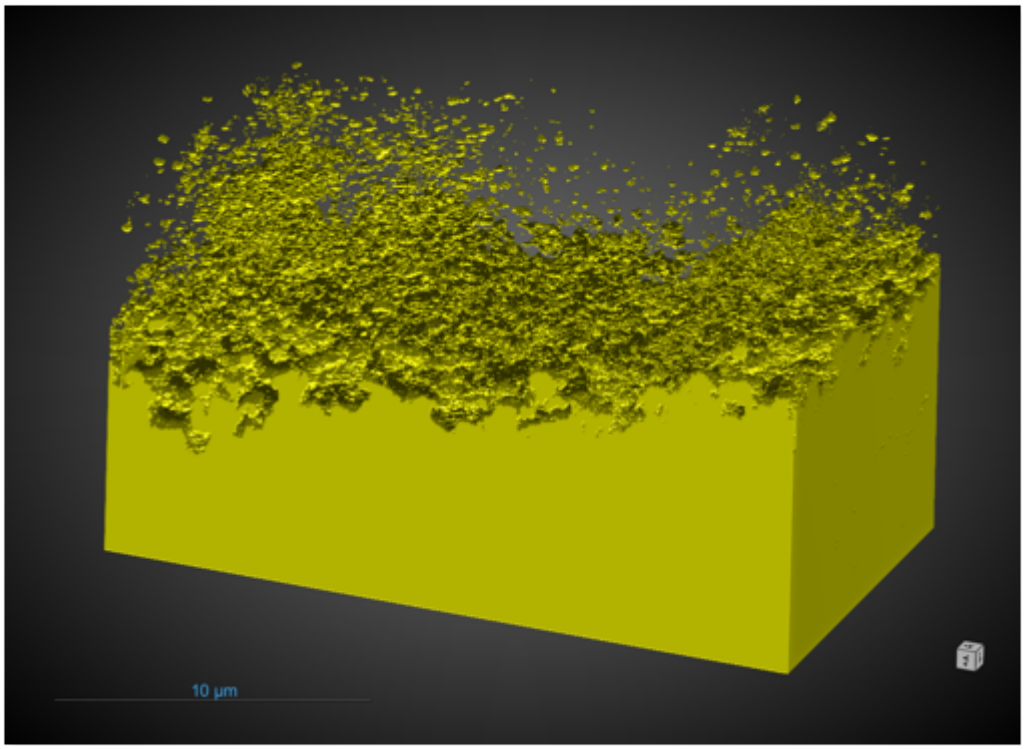

Keywords:

S/TEM, FIB-SEM tomography, bone mineralization

Reference:

1. Macías-Sánchez et al. Adv. Funct. Mater. 32, 2200504 (2022). 2. Buss et al. J. Struct. Biol. 212, 107603 (2020).
3. Shah et al. Bone Reports 13, 100283 (2020).
4. EMS is supported by a Knowledge Generation Project (PID2022-141993NA-I00) funded by MICIU/10.13039/501100011033 and FEDER, UE, and a Juan de la Cierva Incorporación fellowship (IJC2020-043639-I) funded by MCIN/AEI/10.13039/501100011033 and European Union NextGenerationEU/PRTR. Authors gratefully acknowledge financial support from the Max Planck Society.

493

The ultrastructural analysis of plant-microbe interfaces

Isabella Gantner[1], Dr. Julia Buchner[1], Prof. Dr. Andreas Klingl[1]
[1]Plant Development and Electron microscopy, Ludwig-Maximilians-Universität, Munich, Germany

LS-07 (2), Lecture Theater 5, august 28, 2024, 14:00 - 16:00

Background incl. aims
In natural environments, plants share their habitat with various microbes and are colonized by a rich diversity of bacteria and fungi. Over time, different types of plant-microbe interfaces (PMIs) developed to enable interactions between a specific microbe and its host. The most famous PMI are e.g. the symbiosomes in root nodules of legumes, containing nitrogen-fixing bacteria, the arbuscules of mycorrhiza fungi, which are used for the nutrient exchange with the plant and the so called haustoria of some parasitic fungi or oomycetes. Knowing the ultrastructural details of PMIs is central for the biological and functional understanding of plant microbe interactions. This project aims to generate sample preparation methods for TEM and FIB/SEM techniques, visualize PMIs in 2D electron microscopy images and identify their 3D structure.
Methods
Mesorhizobium loti infected plant tissue of Lotus japonicus root nodules was prepared for TEM and FIB-SEM by chemical fixation and embedding in epoxy resin blocks. After ultra-thin sectioning, 2D images were generated with TEM. Furthermore, image stacks were generated by FIB/SEM to enable 3D modeling of the PMI region of interest by structure segmentation.
Results
TEM images of infected root nodule cells confirmed the presence of symbiosomes, which have a plant derived membrane that encloses a peribacteroid space with rod shaped bacteria of Mesorhizobium loti. The 3D model of a symbiosome visualized the arrangement of bacterial cells in the peribacteroid space tightly sourrounded by the symbiosome membrane. With regard to the TEM images, the model revealed further, that the number of bacteria in one symbiosome can be much higher than it was previously assumed by 2D image data of this symbiosis.
Conclusion
Ultrastructural details of plant-microbe interfaces visible in 2D TEM images were verified and analysed by 3D structure construction using FIB/SEM, which gives insight in the complex arrangement of microbes within infected plant cells.

Keywords:

Plant-microbe interaction, TEM, FIB/SEM

677

FIB-SEM and automatic segmentation for investigation of mitochondrial organization in cells of urinary bladder urothelium

Samo Hudoklin[1], Bruno Humbel[2], Manca Žerovnik Mekuč[3], Ciril Bohak[3], Matija Marolt[3], Rok Romih[1]
[1]Institute of Cell Biology, Faculty of Medicine, University of Ljubljana, Ljubljana, Slovenia, [2]Electron Microscopy Facility, University of Lausanne , Lausanne, Swizerland, [3]Faculty of Computer and Information Science, University of Ljubljana, Ljubljana, Slovenia

LS-07 (2), Lecture Theater 5, august 28, 2024, 14:00 - 16:00

Background incl. aims
Mitochondria are the main source of ATP and their ultrastructural features as well as their subcellular distribution depend on cell type and metabolism. In urothelial superficial umbrella cells, ATP is required for the synthesis and delivery of urothelial plaques by fusiform vesicles to the apical plasma membrane where they form a tight permeability barrier between urine and body fluids [1]. On the other hand, mechanical stretch of urothelium during bladder filling promotes ATP production and excretion into extracellular space [2]. ATP activates purinergic receptors on afferent nerves and interstitial cells in the lamina propria and on smooth muscle cells of detrusor. This ATP signalling pathway induces detrusor contraction and thus emptying of the bladder. Mitochondrial structural changes in urothelium were reported in aging organisms and some bladder disorders [3]. Our aims were to preserve the ultrastructure of umbrella cells close to native state in the living organism and to develop a method for the automatic segmentation of mitochondria.

Materials and Methods
Mouse urothelium was high pressure frozen (Balzers HPM010), freeze-substituted (Leica AFS) and embedded in Epon. Ultrastructural features of umbrella cells were examined on ultrathin sections (Philips CM100). The volumetric data from the umbrella cells was generated by Ga-ions milling and imaging in FIB-SEM (Helios NanoLab 650). For automatic segmentation of mitochondria from FIB-SEM data, we propose a pipeline based on a volumetric convolutional neural network with mechanisms that reduce the impact of noisy and inconsistent input data. The main features of the proposed pipeline are a contrast enhancement technique, usage of segmentation masks, and zero-mean convolutions.

Results and Discussion
Ultrathin sections showed numerous flattened fusiform vesicles (Figure 1a) that were composed of two parallel urothelial plaques, which confirmed superior preservation of umbrella cells ultrastructure [4]. Mitochondria with smooth outer membrane were oval to elongate (Figure 1b). Sometimes narrowing was observed (Figure 1c), which point to fissions and fusions of mitochondria [3]. Our approach produced state-of-the-art results for extraction of mitochondria from FIB-SEM volumes [5]. 3D visualization of segmented volumes presented a global distribution of numerous mitochondria within umbrella cells (Figure 1d). Some mitochondria are tubular or globular, but many of them form complex structures (Figure 1e), indicating dynamical changes possibly associated with their various functions [4].

Conclusion
We believe that our approach can be used to better understand the role of mitochondria in normal and in pathological conditions in urothelium as well as other tissues.

Figure 1: Ultrastructure of the umbrella cell and 3D model of their mitochondria. A) Cytoplasm of high pressure frozen – freeze substituted umbrella cell contains mitochondria (M) and tissue specific fusiform vesicles (FV), which could also be organized into stacks (FVs). B) The shape of mitochondria on a two dimensional ultrathin section varied from being oval (Mo) to elongated (Me). C) Narrowing of the mitochondria (arrow). D) Visualization of mitochondria from segmented FIB-SEM volumes (256×256×256 voxels). E) A part of complex mitochondria with a bifurcation and a membrane connection. Bars: 500 nm – A, 250 nm – B, C.

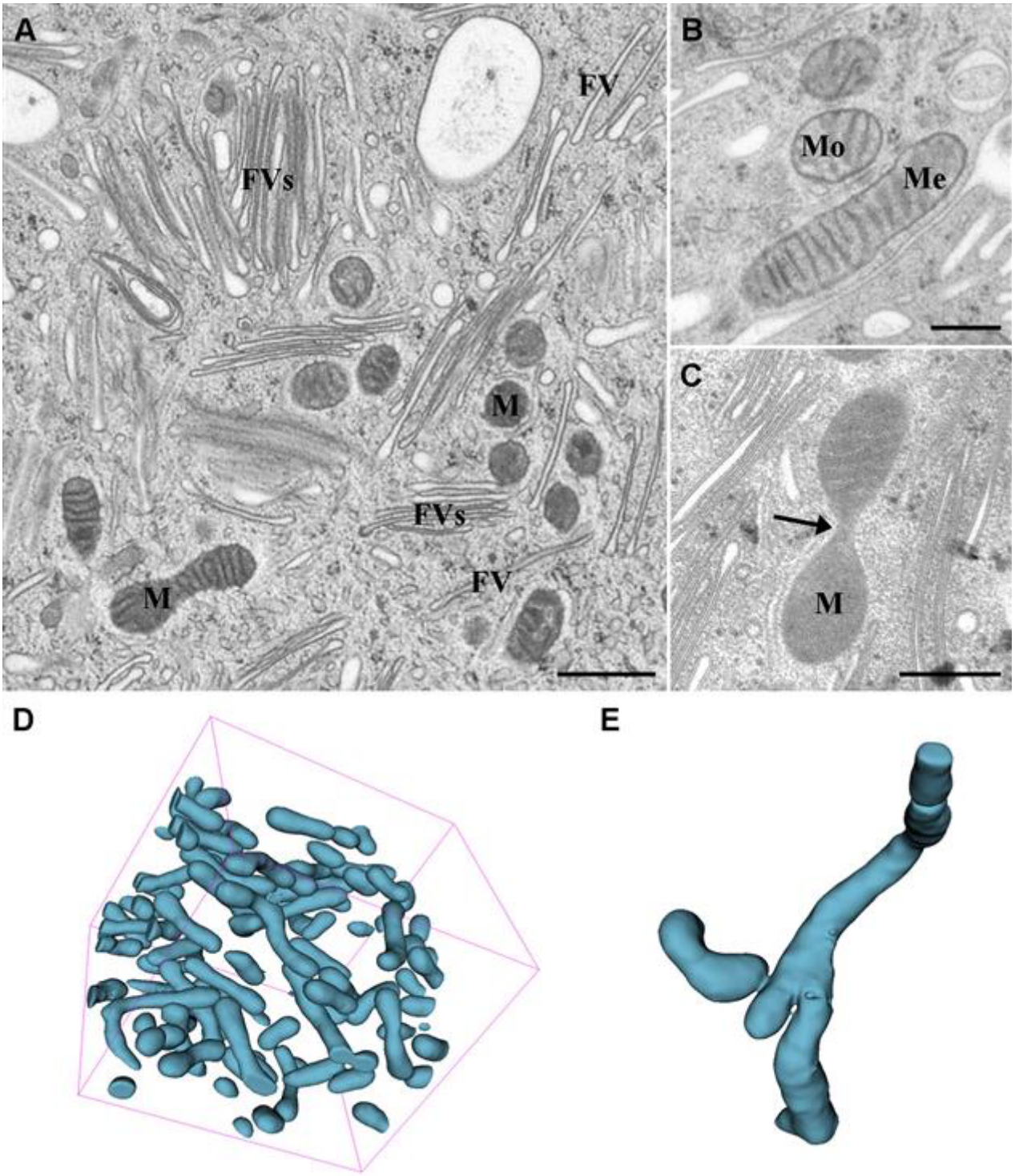

Keywords:

FIB-SEM, segmentation, mitochondria, urothelium, bladder

Reference:

[1] B Wankel et al, Mol Biol Cell 27 (2016), p. 1621.
[2] DAW Janssen, JA Schalken and J Heesakkers, Acta Physiol (Oxf) 220 (2017), p. 201.
[3] FA Kullmann et al, Neurourol Urodyn 38 (2019), p. 572.
[4] S Hudoklin et al, PLoS One 7 (2012), p. e32935.
[5] M Zerovnik Mekuc et al, Comput Meth Progr Biomed 223 (2022), p. 106959.

850

3D TEM and SEM-array tomography of Hailey-Hailey Disease human skin biopsies

Ph.D. Massimo Micaroni[1], P.D. Jens Berndtsson[1], P.D. Rafael Camacho[1], Ph.D. Erin Cocks[1], M.D. Giulio Gualdi[2], Ph.D. Apollonia Tullo[3], Ph.D. Flaviana Marzano[3], M.D. Camilla Marinelli[4], Ph.D. Anna Campanati[5], M.D. Gaetana Lanzi[6], M.D., Ph.D. Manuela Iezzi[7], M.D. Vincenzo Maione[8], M.D., Ph.D. Paolo Amerio[2], Ph.D. Julia Fernandez-Rodriguez[1]
[1]Centre for Cellular Imaging Core Facility, Sahlgrenska Academy, University of Gothenburg, Göteborg, Sweden, [2]Department of Medicine and Aging Science, Dermatology Unit, University "G. d'Annunzio", Chieti-Pescara, Italy, [3]Institute of Biomembranes, Bioenergetic and Molecular Biotechnology – IBIOM, Bari, Italy, [4]UOSD Pathological Anatomy, ASL 2 Abruzzo, "G. Bernabeo" Hospital, Ortona (CH), Italy, [5]Department of Clinical and Molecular Sciences, Dermatology Clinic, Polytechnic Marche University, Ancona, Italy, [6]Medical Genetics Laboratory, Diagnostic Department, ASST-Spedali Civili of Brescia, Brescia, Italy, [7]Department of Neuroscience, Imaging and Clinical Sciences, Pathology Section, University "G. d'Annunzio" Chieti-Pescara, Chieti-Pescara, Italy, [8]Dermatology, ASST-Spedali Civili of Brescia, Brescia, Italy

LS-07 (2), Lecture Theater 5, august 28, 2024, 14:00 - 16:00

Background:
ATP2C1 gene encodes for the secretory pathway Ca2+/Mn2+ pump ATPase type 1 (SPCA1) localizing at the Golgi apparatus. Mutations on the human ATP2C1 gene, causing decreased levels of the SPCA1 expression, have been identified as the cause of the Hailey–Hailey disease (HHD), a rare skin disorder. More than 200 unique mutations have been found, with any hot-spot on the ATP2C1 gene. The HHD patients present raw, blistered areas and lesions, particularly in skin folds where there is moisture and friction. No effective cure exists. Due to reduced expression of functional SPCA1 in HHD patients, altered Ca2+ homeostasis and responsiveness in HHD keratinocytes results in creating an early defect in differentiation process due to a reduced production of involucrin. Keratin expression was also delayed in acantholytic epidermal segments of HHD skin. This results in fragile skin layers. However, no deep investigation at ultrastructural level have been never performed.

Methods:
Advanced gene sequencing has been used to identify mutations on the ATP2C1 gene of HHD patients for this study.
Using volume Scanning Electron Microscopy (SEM)-array tomography we investigated the status of the cell-cell interaction in the epidermis of five different HHD patients. Epoxy resin embedded samples have been sectioned (300nm) using the Powertome-XL ultramicrotome (RMC Boeckler, USA) and serial sections were collected on Kapton tape with an automated ATUMtome collection, and then transferred on Si-wafer support for being imaged in the SEM Gemini 450 (Zeiss, Germany). Sequential images where then managed and over-imposed to generate a 3D model of the cell-to-cell interactions.
Furthermore, using 3D-Transmission Electron Microscopy -tomography we also investigated the alterations in the secretory pathway, with particular focus on the Golgi apparatus, in the keratinocytes (epidermis) and in fibroblasts (dermis). Semi-thin sections (250nm) cut with a UltraCut-UC6 microtome (Leica, Austria) were collected onto formvar-coated copper slot grids and imaged with a Talos L120C Transmission Electron Microscope (TEM) (Thermo Fisher Sc., USA) using motorized tilt-rotate specimen holders. Tilt series datasets were collected at 13500x magnification, using automated data acquisition and image alignment routines as the grids housing the sections were serially tilted over a range of ~130° (±65°) using the microscope Tomo program. Tomograms computed from aligned 2D views were computationally registered and combined in 3D space. All of

the above procedures - along with subsequent image segmentation, surface mesh computation/generation, 3-dimensional visualization and quantitative analysis - were performed using the IMOD software package maintained and distributed by the Boulder Laboratory for 3D Electron Microscopy of Cells at the University of Colorado (Boulder, CO, USA).

Results:
We discovered that interactions among keratinocytes are significantly disrupted, leading to the formation of 'empty spaces' between them. Keratinocytes maintain their tenuous connections primarily through few reamining desmosomes. The overall thickening of the epidermis primarily results from an increase in the number of layers of keratinocytes rather than an expansion of intercellular spaces.
At subcellular level, the Golgi apparatus looks highly swollen, blebbed, and pinched off to larger “bubbles”, rather than vesiculated like previously published in in vitro studies. The overall volume of the Golgi apparatus looks sensitively increased, due to the higher number of the cisternae as well as their volume.
Identification of the heterozygous mutations in the ATP2C1 gene of the 5 patients with HHD revelaed 2 novel mutations (c.2378_2381insTTGT, c.2599A>G), and 3 previously reported nonsense mutation (c.1327C/T, c.1402C>T, c.2554insT).

Conclusions:
We proved a workflow of investigating the overall ultrastructure organization of the human skin in the HHD. For the first time, we observed intracellular morphological organization in the Golgi apparatus of the HHD which is notably different form the previous investigated studies using cell line models. Using SEM array tomography, we also give e deeper view of the general disorganization of the cell-cell contact in the epidermis of the patients. Using combines SEM and TEM methodology we present and feasible approach to deeply investigate poorly studied pathologies, like rare genetic disease.

Keywords:

Hailey-Hailey_Disease; SEM-array-tomography; 3D-TEM- tomography; Golgi_apparatus.

Reference:

N/A

942

Differential axon terminal spread and synapse numbers amongst afferent neurons onto a locust's movement detector

Assoc. Prof. Dr Gerd Leitinger[1], Snjezana Radulovic[1], Dr Erin Cocks[3], Dr Claire Rind[3]
[1]Division of Cell Biology, Histology and Embryology, Gottfried Schatz Research Center, Medical University of Graz, Graz, Austria, [2]Electron Microscopy Research Services, Faculty of Medical Sciences, Newcastle University, Newcastle upon Tyne, UK, [3]Biosciences Institute, Faculty of Medical Sciences, Newcastle University, , Newcastle upon Tyne, UK

LS-07 (2), Lecture Theater 5, august 28, 2024, 14:00 - 16:00

Background incl. aims
The locust giant movement detector neurons, LGMD1 and LGMD2, faithfully signal impending collisions by summing up information about changes in light levels across the compound eye. These changes in light levels are transmitted by trans-medullary afferent neurons that correspond to the thousands of facets of the locust's eye. It is known that the afferent neurons preserve anatomy, so each afferent transmits signals from a defined facet and reaches a defined area on the LGMDs dendritic tree, but anatomical studies of afferent neurons are very rare, with the exception of two full length – reconstructions from a fourth larval instar (reference). In order to detect differences in afferent anatomy, spread of their terminal arbour along the LGMD, and synapse numbers between neighbouring afferents and between the LGMD1 and LGMD2, we are 3D - reconstructing the terminal arbours of afferents of both the LGMD1 and LGMD2.
Methods
Tissue taken from adult locusts is chemically fixed, contrasted and embedded and either one of two 3D Scanning electron microscope methods are employed : either the tissue is serially sectioned within the chamber of a scanning electron microscope and the block face scanned (serial block face SEM), or series of sections are produced using an automated tape collection ultramicrotome (ATUMTome SEM), which are later scanned using Zeiss Atlas software in a Zeiss Gemini SEM.
Results
Surprisingly, in the LGMD2, we found two types of trans-medullary afferent neurons: first, second, other neurons that were rarer had a significantly larger spread of neurites and significantly more synapses among. Retinotopy appeared to be preserved for both neuron types.
Conclusion
The fact that some afferent neurons exhibit larger spread of arbours and more synapses onto the LGMD2 is surprising and has consequences for signal transduction. We assume that for the larger neurons, signal strength is increased at the cost of resolution.
Sponsored by the Austrian Science Fund FWF, grant 32058

Keywords:

LGMD, SBEM, ATUM Tome SEM

Reference:

Wernitznig S et al., J Comp Neurol 2022, 530:518

1244

Volume Electron Microscopy: A Powerful Tool for Studying Embryonic Pineal Organ Development in Birds

Prof. Bogdan Lewczuk[1], Dr Natalia Szyrynska[1], Dr Magdalena Prusik[1]
[1]University Of Warmia And Mazury In Olsztyn, Olsztyn, Poland

LS-07 (2), Lecture Theater 5, august 28, 2024, 14:00 - 16:00

The structure of the pineal organ in birds exhibits significant species variability, with three main types identified: saccular, tubule-follicular, and solid, along with several intermediate forms. The parenchyma of the most commonly observed tubule-follicular type includes the pineal canal, a primary evagination of the neuroectoderm of the diencephalon roof, and numerous follicles. Three types of pinealocytes (receptor pinealocytes, rudimentary-receptor pinealocytes, and secretory pinealocytes) and two types of supporting cells (ependymal-like and astrocyte-like cells) have been identified in the avian pineal organ at the electron microscopy level. However, two-dimensional studies have been insufficient to answer many questions about the spatial organization of pineal parenchyma.

This study utilized volume electron microscopy to investigate the structure of the embryonic pineal organs of the domestic turkey and the domestic goose, chosen for their substantial differences in pineal parenchyma organization. The embryonic turkey pineal organ features follicles with a large lumen surrounded by a thin layer of parenchymal cells, resembling pseudostratified epithelium. In contrast, the pineal parenchyma of goose embryos consists of two distinct parts: follicular areas composed of elongated cells surrounding the follicular lumen and parafollicular areas, which are peripheral to the follicular region and consist of several layers of cells.

The pineal organs of 18-day-old turkey and goose embryos were fixed and contrasted according to a modified protocol by Deerinck et al. (1). Serial block face imaging (SBFI) was performed using 3View 2XP (Gatan, USA) and OnPoint detector (Gatan, USA) operating in EF-SEM Gemini 450 (Carl Zeiss, Germany) with the focal charge compensation system. Stacks of 300-1000 images (15,000 x 15,000 pixels, pixel size 5 nm, section thickness 50 nm) were manually segmented using MIB software (2), and the models were visualized using Amira 3D (Thermo Fisher Scientific, USA).

In the embryonic pineal organ of the domestic turkey, two types of parenchymal cells were identified and classified as embryonic rudimentary receptor pinealocytes and ependymal-like supporting cells. These cells were present in both the pineal follicles and the pineal canal, with structural differences depending on their location. SBFI revealed that rudimentary receptor pinealocytes typically do not contact the basement membrane limiting the follicles and the canal. The basal parts of rudimentary receptor pinealocytes in the follicles had the shape of an inverted cup, with their outer surfaces in contact with ependymal-like supporting cells. In the pineal canal, pinealocytes formed long basal processes that created flattened fragments lying in invaginations of ependymal-like supporting cells. Up to five flat parts of different rudimentary receptor pinealocytes were found in one invagination. Ependymal-like supporting cells had a broad basal portion resting on the basement membrane. Both rudimentary receptor pinealocytes and ependymal-like supporting cells had regular internal organization. In pinealocytes, the organelles were distributed as follows: 1) nucleus in the basal part of cell, 2) accumulation of endoplasmic reticulum cisterns on the upper pole of the nucleus, 3) Golgi apparatus, and 4) mitochondria. The apical protrusion of pinealocytes had a 9+0 cilium and contained endoplasmic reticulum and mitochondria. A key feature of rudimentary receptor pinealocytes was the accumulation of mitochondria in the upper part of the cell, with SBFI showing these mitochondria as elongated and parallel to the cell's long axis. Some mitochondria formed long strands from the cell apex to the perinuclear region. In supporting cells, mitochondria were present throughout the cytoplasm, including the basal process. Secretory pinealocytes and astrocyte-like supporting cells were not found in the turkey pineal organ.

Special attention was given to mitotic cells since precursor cells of pinealocytes and supporting cells have never been described in the avian pineal organ. Cell divisions were more numerous in the pineal canal than in the follicles. Mitotic cells always contacted the canal lumen by short apical processes and had long basal projections ending in numerous fine, parallel-running processes that did not attach to the basement membrane. Daughter cells maintained contact with the lumen and remained connected by a thin cytoplasmic bridge near the canal lumen for an unknown period. These cells lacked a polarized distribution of organelles, leading us to hypothesize that differentiation results in the characteristic distribution of organelles seen in pinealocytes or supporting cells.
Rudimentary receptor pinealocytes in the pineal canal varied in the proportion of cell body length to basal process length. Cells with short bodies and long basal processes exhibited numerous deep invaginations of the nuclear envelope. Occasionally, large parts of the cytoplasm of these pinealocytes, connected to the cell body by a narrow band, were located in the lumen, suggesting that the upper parts of these cells are removed into the lumen. The same process was observed in the pineal follicles. Since undifferentiated precursor cells were not found, we hypothesize that old pinealocytes lose the upper part of their cytoplasm and re-enter the cell cycle.
In the goose pineal organ, follicular areas were mainly composed of cells resembling rudimentary receptor pinealocytes, which created long processes penetrating into the parafollicular areas. Parafollicular areas were primarily composed of embryonic secretory pinealocytes. Supporting cells were exclusively found close to the basement membrane and were largely infrequent due to the parenchyma's poor division by connective tissue, resulting in the majority of cells not contacting the basement membrane. The cells of the parafollicular region formed specific contact sites bordered by tight junctions, created by both cell bodies and cell processes. Secretory pinealocytes showed significant variability in shape and the presence of very long processes. Their cytoplasm often contained three zones with the Golgi apparatus, endoplasmic reticulum, and mitochondria, though not arranged in series.
Funded by the Minister of Science under the Regional Initiative of Excellence Program.

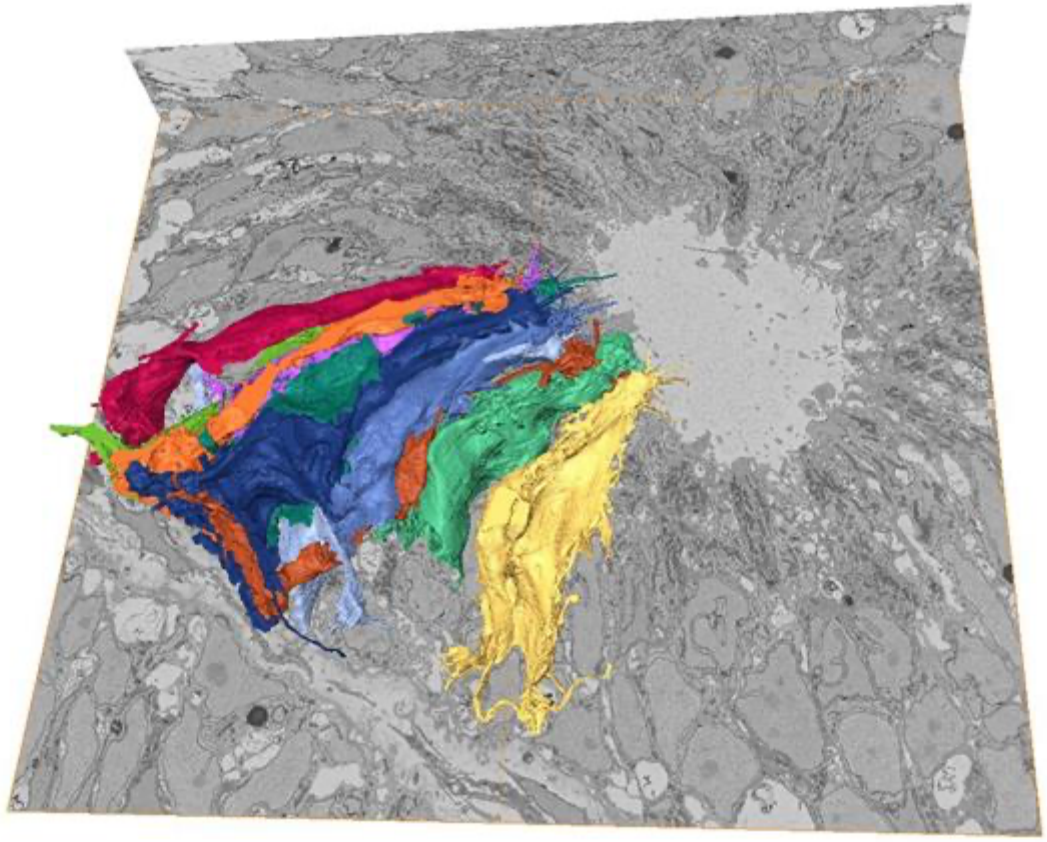

Keywords:

3D-ultrastructure, VEM, pineal organ

Reference:

1. Deerinck TJ, Bushong EA, Thor A, Ellisman MH. NCMIR methods for 3D EM: A new protocol for preparation of biological specimens for serial block face scanning electron microscopy. Microscopy, 2010, 1, 6–8.
2. Belevich I, Joensuu M, Kumar D, Vihinen H, Jokitalo E. Microscopy Image Browser: A platform for segmentation and analysis of multidimensional datasets. PLoS Biology, 2016, 14, e1002340

81

How Euro-BioImaging can support your research with access to the best imaging tools

Johanna Bischof[1]
[1]Euro-BioImaging ERIC, Heidelberg, Germany

Poster Group 2

Advanced imaging technologies are a central technology platform driving research in most disciplines of the life sciences and correlating multiple imaging approaches has become an increased need in many research approaches.

Euro-BioImaging's role in the imaging revolution is to offers all scientists open access to imaging instruments, expertise, training opportunities, and data management services beyond what is available at their home institutions or among their collaborators.

The technologies offered by Euro-BioImaging can be accessed at Euro-BioImaging Nodes, which comprise more than 200 internationally renowned imaging facilities distributed across Europe.

They cover the whole spectrum of biological and biomedical imaging. This includes many facilities that offer imaging methods for characterising chemical and physical composition of samples, and the full spectrum of Electron Microscopy solutions - from cryoET to volumeEM and correlative imaging.

In addition to access to cutting-edge instruments, the Euro-BioImaging Nodes provide expertise, guidance and training on all aspects of the imaging experiment - from experimental design and sample preparation to image analysis services, including on external data.

Euro-BioImaging has a strong commitment to Open Science, working with image data repositories such as the BioImage Archive and EMPIAR, as well as offering image analysis and support with data FAIRification.

All scientists, regardless of affiliation, area of expertise, or field of activity, can benefit from Euro-BioImaging's pan-European open access services and funding for user access is available.

For the technical experts at imaging core facilities, Euro-BioImaging provides a cross-European network and platform for exchange of experience, as well as new training opportunities.

Keywords:

Infrastructure, Open Access, Data Services

832

Exit of different cargoes from the Golgi and their post-Golgi trafficking

Dr. Galina Beznoussenko[1], PhD, MD, Prof. Alexander Mironov[1]
[1]IFOM ETS, The AIRC Institute of Molecular Oncology, Via Adamello 16, 20139, Milan, Italy, Milan, Italy

Poster Group 2

Proteins and lipids are synthesized in the ER, delivered at the Golgi complex, then exit the Golgi complex and finally, delivered toward their final destination. Until now the information about the Golgi-to-plasmalemma transport (GPT) and the formation of Golgi-to-PM carriers (GPC) and their fate is controversial. For a long time, the vesicular model played a role of paradigm for all steps of intracellular transport. However, several years ago it was demonstrated that the transport from the Golgi complex to the plasma membrane (PM) is carried out by irregular GPCs [1,2]. Pathways for different cargoes are not well established. It is not clear whether there is a necessity for the fusion of the post-GC carriers with endosomes. Here, we examined mechanisms of GPT, namely, the three-dimensional structure of post-Golgi carriers, patterns of their exit from the Golgi complex, their transformation during their delivery to the baso-lateral PM and their dependency on the amount of cargo transported and fusion with endosomes.
All reagents, the cells and the cargo synchronization protocols were described in [3]. We studied conventional cargoes: PCI, PCI-GFP (PFP), tsVSVG, tsVSVG-GFP (VFP); ASGPR, albumin, and GFP-albumin (AFP) using STEM and TEM tomography, correlative light electron microscopy (CLEM), high pressure freezing (HPF), immuno-EM, focused ion beam (FIB-SEM).The GPC exit from GC depends on the amount of cargo moving through it. The temperature-sensitive glycoprotein G of vesicular stomatitis virus (VSVG) and procollagen-I (PCI) can also exit from the last two medial Golgi cisternae when a large amount of them is transported, whereas when a small amount of PCI is transported, it passes through the last medial cisterna and the trans-most cisterna (TMC) and then exits the TGN zone. Albumin exits the GC through TMC and TGN, where accumulative large vacuoles are formed. Albumin is enriched in the vacuole(s). Most of these vacuoles contain low concentration of VLDL. Smaller but distinct vacuoles are enriched in VLDL. This vacuole could be connected with the PM through thin tubule. Fusion of GPCs with endosomes and then their subsequent fission is necessary to remove resident Golgi proteins from GPCs and replace SNAREs in GPCs. Using advanced methods of the high-resolution 3D imaging (STEM and TEM tomography, FIB-SEM) after a cryo-immobilization procedure (HPF) has been shown that near the GC and during their passage to the PM, GPCs are always connected with at least one GC/TGN/endosome structure. The exchange of SNARE proteins ensures the subsequent fusion of GPCs with the PM. Thus, the kiss-and-run model is the most powerful model for the explanation of GPT.

Keywords:

Golgi, post-Golgi, transport, 3DEM, tomography

Reference:

1. Polishchuk RS, Polishchuk EV, Marra P, Alberti S, Buccione R, Luini A, Mironov AA (2000) Correlative light-electron microscopy reveals the tubular-saccular ultrastructure of carriers operating between Golgi apparatus and plasma membrane. J Cell Biol 148: 45-58
2. Polishchuk EV, Di Pentima A, Luini A, Polishchuk RS (2003) Mechanism of constitutive export from the Golgi: bulk flow via the formation protrusion and en bloc cleavage of large trans-Golgi network tubular domains. Mol Biol Cell 14: 4470–4485
3. Beznoussenko GV, Bejan A Iu, Parashuraman S, Luini A, Kweon HS, Mironov AA (2022) The diffusion model of intra-Golgi transport has limited power. Int J Mol Sci 23.

835

Investigating Bone Microstructure with ATUM-SEM: Implications for Pathological Conditions

Ph.d Valeria Vistoso[1], Dr. Tom Fertè[1], Dr. Federica Buccino[2], Professor Laura Maria Vergani[2], Professor Ovidiu Ersen[1], Professor Adele Carradò[1]
[1]Institut de physique et chimie des Matériaux de Strasbourg, University of Strasbourg, Strasbourg, France, [2]Department of Mechanical Engineering, Politecnico di Milano, Milan, Italy

Poster Group 2

Background incl. Aims
Bone tissue's hierarchical structure is pivotal for various mechanical, biological, and chemical processes essential to health. However, the mechanical properties of bones are susceptible to deterioration, leading to an increased risk of fragility fractures associated with ageing, vitamin D deficiency, and bone density pathologies, such as osteoporosis [1]. The prevalence of these chronic illnesses, coupled with rising life expectancy, has become a significant public health concern. Additionally, the COVID-19 pandemic potentially exacerbates bone health issues, leading to decreased bone mass and strength in long-term hospitalised patients [2]. Bone fractures result in significant psycho-social and economic burdens, yet current understanding is limited to macro- and mesoscale levels. The challenge lies in comprehending the mechanobiological perspective at the multiscale level (between the mm and nm ranges). This knowledge gap, coupled with the influence of other intricate structural parameters, underscores the need for advancements in research tools and technical approaches.

Methods
Automated Tape Collecting Ultramicrotome Scanning Electron Microscopy (ATUM-SEM) has been introduced as an effective method for capturing high-quality images of hard tissues [3]. In this case study, the choice of using ATUM-SEM was driven by the need for a non-destructive approach that could enable the examination of the largest possible volume. The method was chosen for its flexibility, which allows cutting slices sections with a chosen thickness while preserving all of them for subsequent observations. Despite a thorough literature search, no suitable protocol was found to prepare human trabecular bone compatible with the ATUM-SEM-based approach. Consequently, it was determined that the best course of action was to utilise the same workflow previously used in the analysis of biological samples, with some adapted modifications made on a case-by-case basis. Trabecular bone samples from female and male patients diagnosed with different clinical conditions, namely osteoporotic, COVID-19, and a healthy control group, were evaluated. The specimens were processed by cutting them into macroscopic shapes appropriate for applying the ATUM-SEM approach, followed by careful cleaning and dehydration to improve their embedding in the resin. The resin embedding process was optimised for efficient sectioning, and a good trimming and polishing of the face of the specimen block was crucial for a stable section collection protocol. Slices, with thickness ranging from 300 nm to 400 nm, were collected onto Kapton tape using an Ultramicrotome. The imaging workflow that was utilised to reconstruct the acquired volume was managed using Atlas 5 Array tomography software and Fiji. Creating a 3D representation requires accurate positioning of images in a virtual volume through registration. The alignment of the image stacks was accomplished using the TrakEM2 plug-in. Finally, Data visualisation is achieved using the 3D volume rendering present in Fiji.

Results

The ATUM-SEM data sets have yielded both qualitative and quantitative analyses, revealing distinctions in lacuna size and shape between osteoporotic and non-osteoporotic cases. Specifically, the osteoporotic and COVID-19 lacunae were larger, less stretched, and more rounded, with the average dimensions ranging from 6.12 µm x 12.27 µm x 10.8 µm and 7.17 µm x 20.96 µm x 6.9 µm, respectively. In the femoral head, lacuna volume exhibited internal variability, with osteoporotic and COVID-19 cases showing pronounced differences compared to healthy specimens (Figure 1). In the femoral head, the volume of the lacunae presents internal variability, ranging from 26% in healthy specimens to 14% in osteoporotic ones and 18% in COVID-19 patients. The volume difference is more pronounced when comparing the physiological state with the two pathological conditions. The volume of the osteoporotic lacuna is approximately 39% larger than the healthy sample, while the volume of the COVID-19 lacuna is around 53%. The complexity of the COVID-19 pathology requires further cellular-level studies to isolate its direct effects on bone microstructure and understand lacunar alterations among different variants, even if the possibility of bone micro-structural deterioration due to COVID-19 is proven [4]. The results of increased lacunar sphericity in osteoporotic subjects are consistent with other research works demonstrating that lacunar stretch is reduced in patients affected by this pathology [4]. Nevertheless, image segmentation and processing still need to be improved for quantitative analysis, demanding improvements in automated segmentation routines. While there are ongoing debates regarding the impact of age on bone microstructure, the study has identified age-related variations in the characteristics of canaliculi and lacunae.

Conclusion

This study highlights the importance of examining bone microstructure at finer levels to understand bone health and disease. ATUM-SEM provides high-resolution imaging and detailed analysis of bone microstructures, leading to better diagnosis and treatment of bone-related disorders. Exploring ATUM-SEM's clinical applications for early bone pathology detection shows promise and may lead to targeted therapies. These future directions in ATUM-SEM analysis of bone pathologies pave the way for enhanced research and clinical applications in the field, leading to a future where targeted interventions can mitigate the burden of bone-related disorders

Figure 1: The following illustrations depict an example of the structure of a single lacuna with a partial reconstruction of the canaliculi system for each specimen analysed. (a) healthy specimen, (b) osteoporotic specimen, (c) COVID-19 specimen.

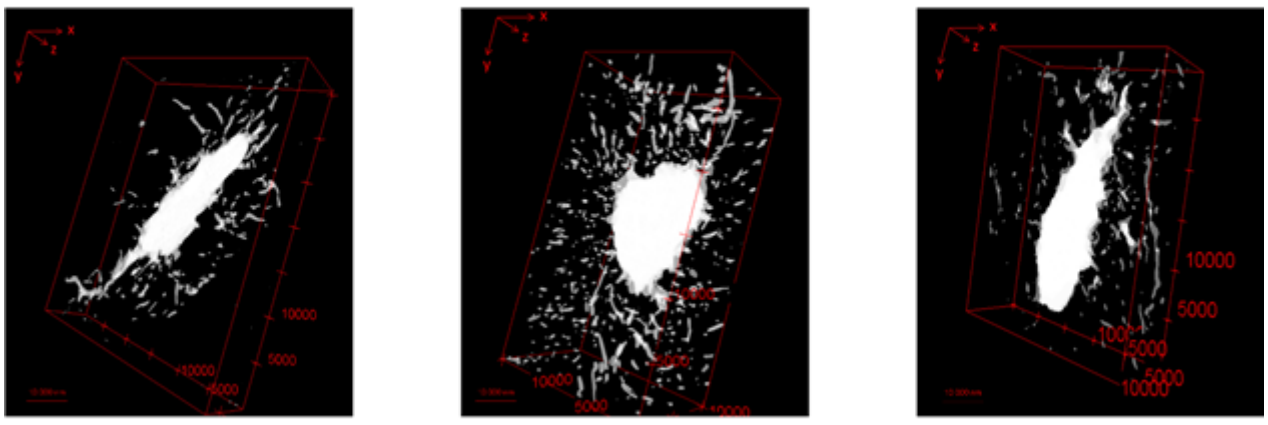

Keywords:

Bone-microstructure, Osteoporosis, Lacunae-canaliculi-system, ATUM-SEM, 3D-imaging.

Reference:

[1] Natacha Rosa et al. From mechanical stimulus to bone formation: a review. Medical engineering & physics, 2015.
[2] Sara Cromer and Elaine Yu. Challenges and opportunities for osteoporosis care during the covid-19 pandemic. The Journal of Clinical Endocrinology & Metabolism, 2021.
[3] Patricia Goggin et al. Development of protocols for the first serial block-face scanning electron microscopy (SBF-SEM studies of bone tissue. Bone, 2020.

[4] Federica Buccino et al. Osteoporosis and COVID-19: Detected similarities in bone lacunar-level alterations via combined AI and advanced synchrotron testing. Materials & Design, 2023

876

Ultrastructural analysis of liver injury and regeneration after microcystin-LR intoxication in whitefish

PhD Natalia Szyrynska[1], Bogdan Lewczuk[1], Maciej Wozny[2], Pawel Brzuzan[2]
[1]Department of Histology and Embryology, Faculty of Veterinary Medicine, University of Warmia and Mazury in Olsztyn , , Poland, [2]Department of Environmental Biotechnology, Faculty of Geoengineering, University of Warmia and Mazury in Olsztyn, , Poland

Poster Group 2

Microcystin-LR (MC-LR) is a cyanobacterial hepatotoxin that is produced in large quantities during algal blooms. It poses a health threat to aquatic organisms in particular, but also to non-aquatic animals because it contaminates drinking water. MC-LR is an extremely dangerous toxin, as the LD50 for intraperitoneal administration in mice is only 25–150 µg/kg body weight (1). MC-LR acts on mature hepatocytes expressing organic anion transporting polypeptides, which are responsible for the uptake of the toxin, but not on cells of the bile duct system (2). Our previous study has shown that the high dose of MC-LR (100 µg/kg body weight) caused severe injury of hepatocytes at the beginning of the post-exposure period, while the low dose (10 µg/kg body weight) caused less, probably reversible, hepatocytes damage and its effects were observed later in the post-exposure period in whitefish (3). Transmission electron microscopy (TEM) showed that the main targets for the cytotoxic effects of MC-LR were endoplasmic reticulum, cytoskeleton, and chromatin. The high dose of toxin induced massive hepatocyte death within 24–48 hours after administration. Histological examinations showed that the liver regenerated after this damage. Unfortunately, the samples for ultrastructural examinations were not collected during the regeneration phase, so that the details of this process remain unknown. The aim of the present study was to characterize the processes of liver injury and regeneration after single administration of a high dose of MC-LR to whitefish. For TEM-like imaging of large sample areas, we used highly sensitive, high resolution detection of backscattered electrons (BSE) in a field-emission scanning electron microscope (4).
Juvenile whitefish (29.9±1.6 g) were anesthetized in MS-222 solution and received an intraperitoneal injection of MC-LR solution (100 µg/kg body weight) or phosphate buffer saline (control). Randomly selected fish were euthanized by immersion in overdosed MS-222 solution 1, 2, 6, 9 and 14 days after administration of the toxin or saline. Liver samples were immediately fixed in a mixture of 1 % paraformaldehyde and 2.5 % glutaraldehyde in 0.2 M phosphate buffer for 2 hours at 4°C, then washed and post-fixed in 2 % osmium tetroxide for 2 hours. After dehydration, the samples were embedded in Epon 812. Ultrathin sections were cut using the PT3D PowerTome ultramicrotome with ASH2 (Boeckeler Instruments, USA), placed on silicon wafers, and contrasted with uranyl acetate and lead citrate. Sections were imaged using a SenseBSD backscatter electrons detector in SEM Gemini 450 at 1.4 kV, controlled by Atlas 5 software (Carl Zeiss, Germany).
The liver parenchyma of the control fish consisted of polygonal hepatocytes arranged in cords running along the capillary blood vessels. The vascular domains of hepatocytes were covered by very long, irregular microvilli. Hepatocytes were characterized by a euchromatin-rich nucleus, long, parallel cisterns of granular endoplasmic reticulum, a well-developed smooth endoplasmic reticulum and numerous mitochondria, usually with electron-dense matrix. Lysosomes were mostly located close to the lateral domain. The glycogen particles and lipid droplets were infrequently noted. In the samples taken 24 hours after the toxin administration, hepatocytes had lost their polygonal shape and were oval or irregular. Oval cells usually had a low electron density, while irregular cells had a moderate or high electron density. Microvilli were absent both on the vascular domain and on the cell membrane creating the bile canaliculi. The endoplasmic reticulum was present in the form of large, differently shaped vesicles that filled the entire cytoplasm. The nuclear envelope was usually dilated. Mitochondria remained unchanged in majority of cells. The lipid droplets with different

diameters were frequently observed. Some hepatocyte nuclei showed chromatin clamping. The next day, 48 hours after MC-LR administration, the majority of hepatocytes, usually of high or moderate electron density, showed prominent condensation and marginalization of chromatin. Mitochondria in these cells were swollen with electron lucent matrix or condensed with electron dark matrix. Oval, electron lucent necrotic cells and typical, round, electron-dense apoptotic cells were also observed. Some areas of the liver parenchyma contained cell debris. Despite the severe damage of hepatocytes, the capillaries retained their continuity, but cell debris was sometimes found in the blood vessels. Single macrophages were also found. On day 6 after exposure, the liver parenchyma contained numerous phagocytes located between cell debris and remnants of apoptotic cells. The cells of the bile ducts formed short cords with numerous intercellular canaliculi. The apical parts of these cells were filled with keratin filaments. The cords of epithelial cells originating the bile ducts were much more numerous on the day 9 after intoxication. The cells forming the cords were rich in cytoplasm, which contained well-developed rough endoplasmic reticulum and Golgi apparatus as well as numerous myelin-like figures. Mitoses were observed in these cells. The liver parenchyma on day 14 after administration of the toxin consisted mainly of immature hepatocytes with well-developed endoplasmic reticulum, numerous mitochondria and glycogen particles. Hepatocytes were poorly equipped with microvilli, both in the vascular domain and in the bile canaliculi. Like the epithelial cells of the bile ducts, hepatocytes showed an accumulation of keratin filaments under the cell membrane of the biliary pool. Macrophages were observed between hepatocytes.
In conclusion, three phases can be distinguished in the course of changes in liver induced by a single administration of the sublethal dose of MC-LR: damage of hepatocytes, infiltration of macrophages and phagocytosis of cellular debris, and proliferation of progenitor cells located in the bile duct system and their differentiation into hepatocytes. The neighbouring hepatocytes differ in their response to MC-LR and take the pathway to apoptotic death or necrosis. Macrophages remain in the regenerating liver for a long time, suggesting their role in the control of transformation of liver progenitor cells into hepatocytes. Liver regeneration after damage of the majority of hepatocytes occurs via the proliferation and differentiation of progenitor cells located in the bile duct system. Our results have also showed that the highly sensitive detection of BSE is an extremely powerful technique for study of tissue ultrastructure.
Funded by the Minister of Science under the Regional Initiative of Excellence Program and National Science Centre of Poland (2016/21/B/NZ9/03566).

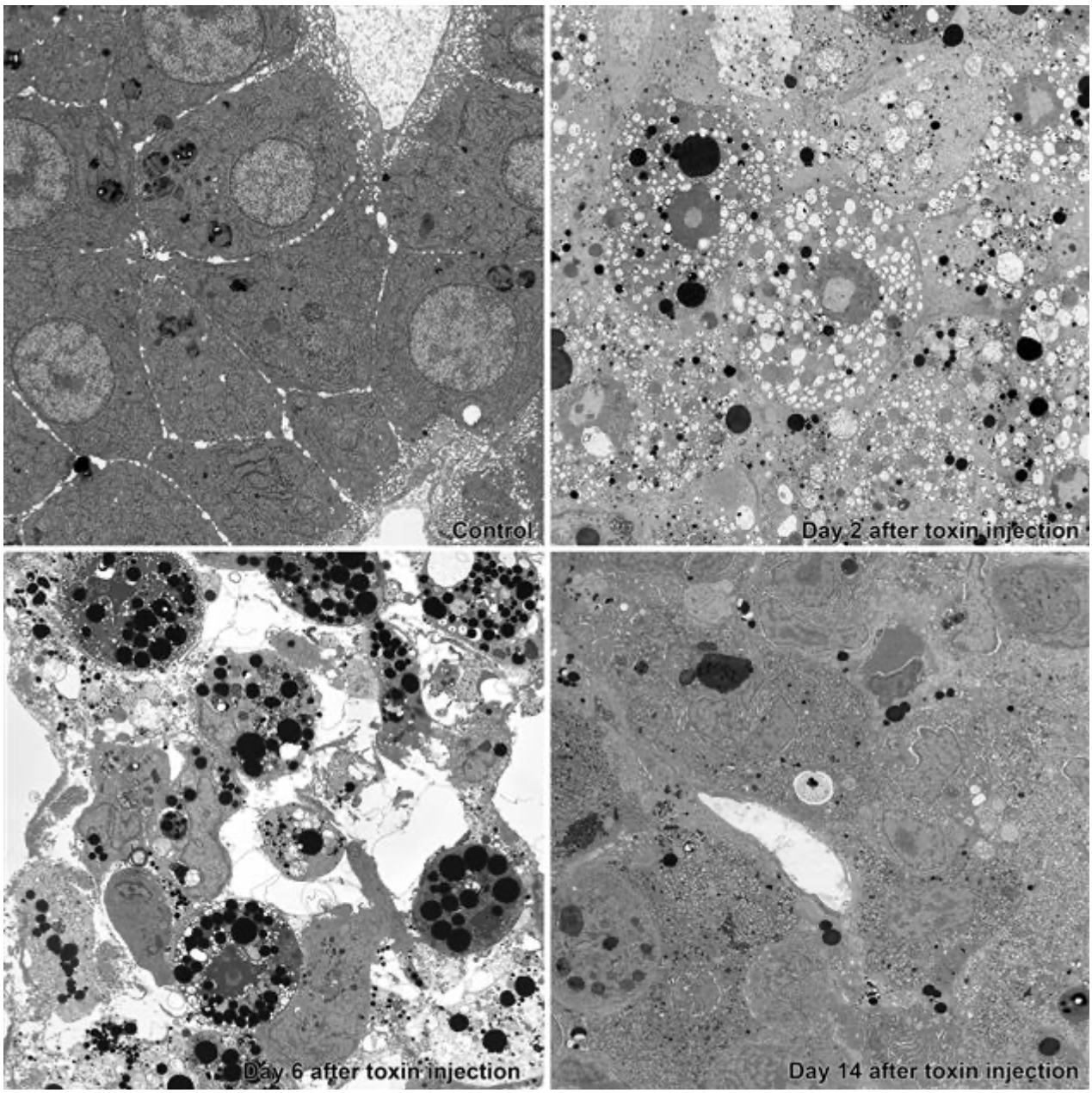

Keywords:

whitefish, toxin, liver, ultrastructure

Reference:

1. Yoshida T., Makita Y., Nagata S., Tsutsumi T., Yoshida F., Sekijima M., Tamura S., Ueno Y. Acute oral toxicity of microcystin-LR, a cyanobacterial hepatotoxin, in mice. Natural Toxins, 1997, 5, 91-5.
2. Shi L., Du X., Liu H., Chen X., Ma Y., Wang R., Tian Z., Zhang S., Guo H., Zhang H. Update on the adverse effects of microcystins on the liver. Environ Research, 2021, 195, 110890.
3. Woźny M., Lewczuk B., Ziółkowska N., Gomułka P., Dobosz S., Łakomiak A., Florczyk M., Brzuzan P. Intraperitoneal exposure of whitefish to microcystin-LR induces rapid liver injury followed by regeneration and resilience to subsequent exposures. Toxicology and Apply Pharmacology, 2016, 313, 68-87.
4. Lewczuk B., Szyryńska N. Field-Emission Scanning Electron Microscope as a Tool for Large-Area and Large-Volume Ultrastructural Studies. Animals, 2021, 11, 3390.

891

Three-dimensional ultrastructure of ovine pinealocytes

Prof. Bogdan Lewczuk[1], Dr Natalia Szyrynska[1]
[1]Department of Histology and Embryology, Faculty of Veterinary Medicine, University of Warmia and Mazury in Olsztyn, , Poland

Poster Group 2

The pineal gland via secretion of melatonin plays an important role in the regulation of processes that occur in the daily and seasonal rhythms. Significant differences between species have been described in ultrastructure of the pineal gland in mammals. Mammalian pinealocytes differ mainly in the structure of endoplasmic reticulum and mitochondria as well as in the presence of clear and granular vesicles, lipid droplets, vacuoles, dense bodies and synaptic ribbons. In addition, depending on the species, both capillary vessels with a continuous wall and those with pores were found. The organization of the pineal parenchyma is very complex due to the presence of numerous cell processes. Based on classical two-dimensional transmission electron microscopy, mammalian pinealocytes have been described as cells with the main process running towards the capillary vessels and forming the bulbous ending close to or inside the perivascular space, and with some small, short processes. The improvement of backscattered electron imaging and the development of volume electron microscopy open the way for a more reliable and precise characterization of the pineal gland structure.
The pineal glands of domestic sheep aged 9 months were prepared according to the modified protocol of Deerinck et al. (1). For high-resolution imaging of the large sample areas, ultrathin sections were cut with the PT3D PowerTome ultramicrotome with ASH2 (Boeckeler Instruments, USA) and placed on silicon wafers. Some sections were additionally contrasted with uranyl acetate and lead citrate. The sections were imaged using the SenseBSD backscatter electron detector in SEM Gemini 450 at 1.4 kV, controlled by Atlas 5 software (Carl Zeiss, Germany). Serial block face imaging was performed with the 3View 2XP and the OnPoint detector (Gatan, USA) operating in SEM Gemini 450 with the focal charge compensation system (Carl Zeiss, Germany). Stacks of 1000 - 2000 images (15,000 x 15,000 pixels, pixel size 5 nm, section thickness 50 nm) were segmented manually and automatically using Microscopy Image Browser software. The models were visualized with Amira 3D (Thermo Fisher Scientific, USA).
The imaging of ultrathin sections on silicon wafers allowed ultrastructural visualization of large sample areas (1 x 2 mm) with a resolution 5 nm/pixel. The pineal gland capsule and the connective tissue trabeculae running from the capsule into the gland were completely separated from the parenchyma by the basement membrane. They contained blood vessels and nerve fibers. The parenchyma comprised pinealocytes and glial cells, mainly astrocytes. The cell bodies of pinealocytes formed small groups. Similar groups formed cell bodies of astrocytes. The large areas of parenchyma between the cell bodies were filled with the cellular processes, which in most cases contained intermediate filaments. Processes of pinealocytes, which distinguished by the presence of microtubules, were much less frequently found in these areas. There were also round or oval structures ranging in size from 0.2 to 5 µm filled with fine granular material of low electron density, the origin and character of which cannot be recognized on 2D images. The capillary vessels running through the parenchyma were surrounded by a thick layer of collagen fibers separated from the rest of the parenchyma by the continuous basement membrane. From the outside, this membrane was covered by ending of astrocytes.
The three-dimensional reconstruction of the pineal parenchyma revealed that pinealocytes of the sheep consisted of an irregularly shaped cell body and two types of processes: “large” processes and “small” processes. The surface of the cell body formed conspicuous invaginations to adapt to the numerous processes of other cells running in its vicinity. The shape of the cell body and the

localization of the nucleus within it differed greatly between pinealocytes. The cell body comprised the Golgi apparatus, which consisted of 3 – 6 dictyosomes, a very dense network of tubules and cisternae of endoplasmic reticulum, numerous elongated mitochondria and a few lipid droplets. The number of “large” processes growing out of the cell body varied between 3 and 5. These processes often divided dichotomously into secondary processes, which form further branches. The “large” processes consisted of alternating wider and narrower parts. The wider parts, with a size of 1 – 3 µm, comprised large mitochondria, tubules of endoplasmic reticulum, vesicles and microtubules. Narrower parts, with a size of 0.2 - 1 µm, contained only a few tubules of endoplasmic reticulum and microtubules. The “small” processes grew out of the cell body in a number of 3 - 10. They form branches and contain tubules of endoplasmic reticulum, vesicles, microtubules and sometimes small mitochondria. The pinealocyte processes did not form bulbous endings.

The results obtained indicate that the descriptions of ovine pinealocytes based on transmission electron microscopy (2) should be revised. These cells have a few “large” processes of similar size that form branches, instead of the main process. The processes of ovine pinealocytes did form neither bulbous endings nor any ending close to perivascular spaces. It appears that the wider parts of pinealocyte processes play an important role in melatonin synthesis and secretion, increasing the area in which a pinealocyte realises the hormone. Our morphological observations are consistent with previous physiological data showing that melatonin concentration in cerebrospinal fluid is about 20-fold higher than in blood and that it is higher in the pineal recess than in the ventral part of the third ventricle (3). The differences in melatonin concentrations suggest that pineal hormone is released from the ovine pineal gland to the third ventricle in greater quantities than to the blood. Taken together, the morphological and biochemical data seem to indicate that the ovine pinealocytes realize melatonin into the extracellular space around the cell body and the cell processes, from where this lipophilic hormone enters the third ventricle and the intrapineal blood vessels, which are separated from the parenchyma by the blood-brain barrier. Comparison of the results of 3D studies on rat (4) and ovine pinealocytes shows that the differences between the species may be even more pronounced and important than previously thought based on 2D data.

Funded by the Minister of Science under the Regional Initiative of Excellence Program.

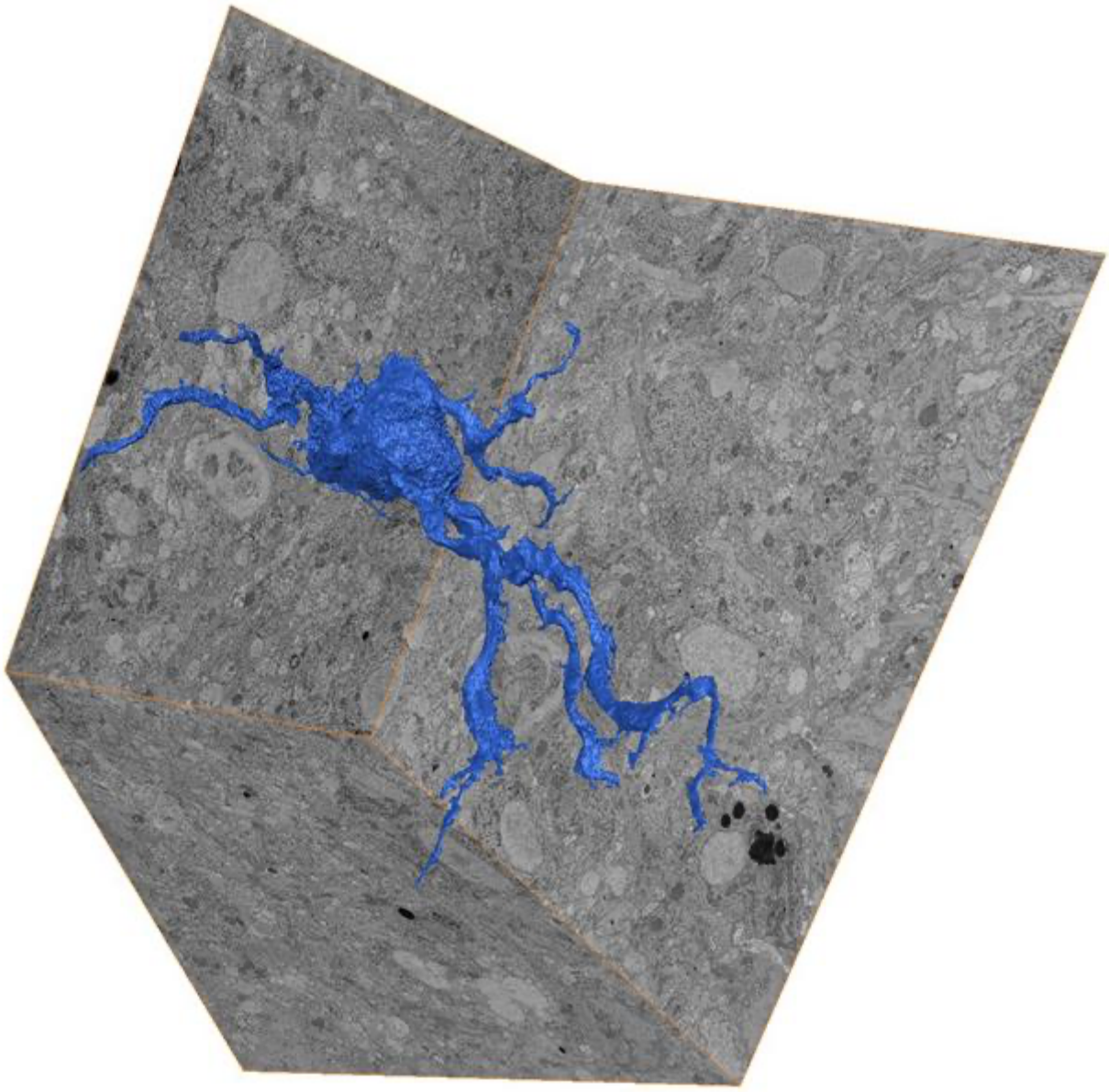

Keywords:

pinealocyte, pineal, ultrastructure, vEM, SBF-SEM,

Reference:

1. Deerinck TJ, Bushong EA, Thor A, Ellisman MH. NCMIR methods for 3D EM: A new protocol for preparation of biological specimens for serial block face scanning electron microscopy. Microscopy, 2010, 1, 6–8.
2. Anderson E. The anatomy of bovine and ovine pineals. Light and electron microscopic studies. Journal of Ultrastructure Research, 1965, 28, Suppl 8, 1-80.
3. Tricoire H, Malpaux B, Møller M. Cellular lining of the sheep pineal recess studied by light-, transmission-, and scanning electron microscopy: morphologic indications for a direct secretion of melatonin from the pineal gland to the cerebrospinal fluid. Journal of Comparative Neurology, 2003, 456, 39-47.
4. Møller M, Midtgaard J, Qvortrup K, Rath MF. 3-Dimensional Ultrastructural Analysis of the Rat Pinealocyte: Presence of Secretory Bulbous Projections Delineated from the Cell Body by Junctional Complexes. Neuroendocrinology, 2024, 114, 291-301.

917

Simple and efficient three-dimensional reconstruction method of plant cells using transmission electron microscope

Ms. Haruka Aoki[1], Ms. Mizuki Matsuzaki[1], Mr. Hideo Nishioka[1], Ms. Chieko Hamamoto[1]
[1]JEOL Ltd., Akishima, Japan

Poster Group 2

Serial section transmission electron microscopy (ssTEM) is a vital technique in Volume Electron Microscopy (vEM) for unveiling fine structures of cells and tissues in three dimensions (3D). While the ssTEM provides superior X and Y resolution compared to other vEM, it is a challenge to acquire wide field of view images. Conventional mesh grids, for instance, often obscure the desired field of view with mesh bars. Even single-hole grids without bars, the support membrane remains susceptible to tearing and wrinkling, risking the loss of information. To address these challenges, we employed SiN Window Chip [1] for ssTEM. SiN Window Chip has no bars, ensuring uninterrupted observation without any missing information. In addition, its support membrane, made of high-strength silicon nitride film, minimizes the risk of tearing, distinguishing it from single-hole grids. We collected approximately 50 sections, each 70 nm in thickness, onto each of the five SiN Window Chips, resulting in a total of about 250 serial sections. The serial section images of a carrot leaf cell were obtained with a sample holder capable of simultaneously mounting multiple SiN Window Chips. For data acquisition, we used a new 120-kV transmission electron microscope (JEM-120i) equipped with a pole piece that provides high contrast. We attempted to undertake a segmentation analysis of organelles from the 177 TEM images.
Segmentation for annotating regions of interest continues to rely largely on manual methods. This task requires extensive time and effort, a challenge commonly encountered in other vEM as well. To streamline this task, we used convolutional neural networks (CNN) [2], a subtype of deep learning. Only a small number of images were required as training data; chloroplasts were manually segmented from just five images of 512x512 pixels (18.4 nm/pixel). Subsequently, a model was trained using deep learning based on these training data, and chloroplasts were inferred from all TEM images. The entire process, from model training to inference, took only an hour. In contrast, if performed manually, this process would take several weeks. As a result of 3D reconstruction of a cell body and chloroplasts, we gained insights into their shape, distribution, and volume.
Performing 3D reconstruction based on the inference results obtained through deep learning enables streamlined analysis of the shape and distribution of the target tissue. Additionally, the trained model can be applied to different serial section data. We successfully employed the model to other fields of view obtained from the same specimen. Therefore, we anticipate that this method can also reduce the time required for training data creation.

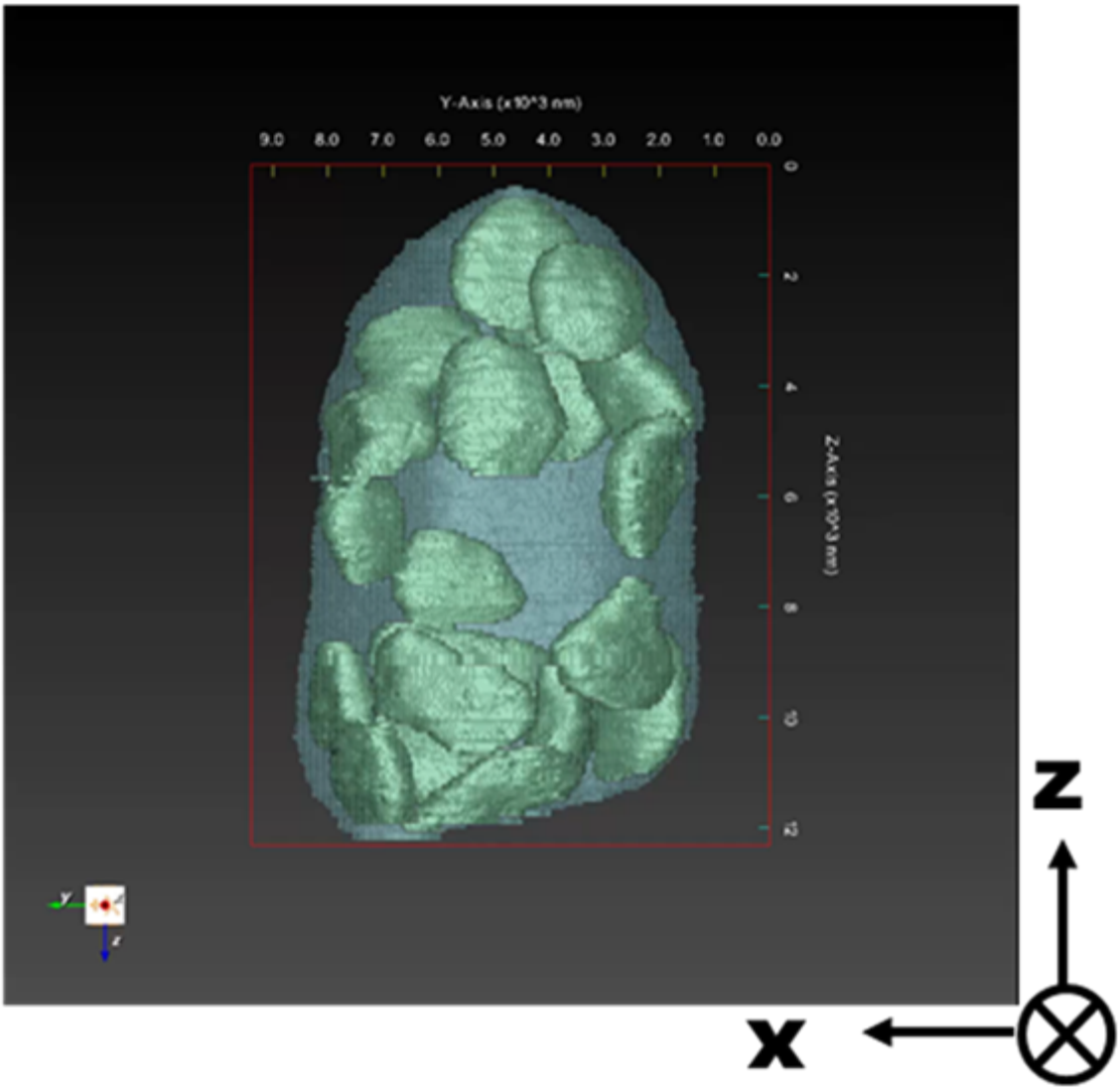

Keywords:

ssTEM
vEM
CNN
Deep Learning

Reference:

[1] Y. Konyuba et al., Microscopy, 67, 367-370 (2018)
[2] K. Konishi et al., Microscopy, 70, 526-535 (2021)

956

Sample preparation for correlative light, soft X-ray tomography, and cryo FIB-SEM imaging of biological cells

Director Imaging Applications Sergey Kapishnikov[1], Maryna Kobylynska[2,3], Prof. Roland A. Fleck[2,3], Malene Fog Lihme Olsen[4], Prof. Poul Erik Jensen[4], Dr Kenneth Fahy[1], Dr Paul Sheridan[1], Dr William Fyans[1], Dr Fergal O'Reilly[1,5,6], Tony McEnroe[1]
[1]SiriusXT Ltd., Dublin, Ireland, [2]Randall Centre for Cell and Molecular Biophysics, King's College London, London, United Kingdom, [3]Centre for Ultrastructural Imaging, King's College London, London, United Kingdom, [4]Department of Food Science, University of Copenhagen, Copenhagen, Denmark, [5]School of Physics, University College Dublin, Dublin, Ireland, [6]School of Biology and Environmental Sciences, University College Dublin, Dublin, Ireland

Poster Group 2

In this collaborative endeavor between SiriusXT and King's College London (KCL), we present our efforts to refine high-pressure freezing (HPF) protocols tailored to facilitate correlative imaging workflows integrating cryo-fluorescence microscopy, lab-based soft X-ray cryo-tomography (SXT), and cryoFIB-SEM for high-resolution three-dimensional (3D) imaging of biological cells. This refined protocol is followed by correlative light fluorescence, SXT, and FIB-SEM studies of biological cells, aiming to compare sample quality vitrified by plunge freezing and high-pressure freezing. Our motivation stems from the persistent uncertainty surrounding the efficacy of plunge freezing in adequately vitrifying thicker cellular components for high-resolution imaging purposes.
The primary objective of our study is to develop strategies to regulate ice thickness in high-pressure frozen samples, making them suitable for correlative imaging by light, SXT, and cryo-FIB-SEM techniques. Subsequently, we employ correlative imaging to investigate regions of interest, initially utilizing light fluorescence and soft X-ray tomography, followed by identification of regions of interest and further imaging of these regions using cryo FIB-SEM. We also compare the quality of frozen samples between high-pressure and plunge-frozen specimens. For our study we use two distinct biological organisms: the nannochloropsis microalgae and single-cell flagellate eukaryotes of the Euglena genus.
Optimal ice thickness for direct imaging by SXT without the need to thin the sample typically falls below fifteen micrometers, a threshold often exceeded by the conventional HPF "waffle" method, resulting in ice thicknesses around 20-25 micrometers. However, through modifications to the freezing procedure - such as liquid wicking and removal of planchettes spacer - we demonstrate the achievement of HPF ice thickness as low as 5-15 micrometers across significant fractions of the grid area.
This improvement eliminates the need to thin high-pressure frozen samples for SXT imaging. Using the lab-based SXT-100 for rapid 3D imaging of large areas with resolutions of 50-60 nm full-pitch, this approach enhances the throughput of cryo FIB-SEM imaging of high-pressure frozen samples by streamlining the process of identifying regions of interest for higher resolution imaging, albeit at a significantly slower imaging pace by cryo FIB-SEM.

Keywords:

SXT, cryoFIB-SEM, correlative microscopy, tomography

Reference:

We acknowledge funding from the European Union's Horizon
2020 Research and Innovation programme (No. 101120151, project CLEXM and No. 101017116, project CoCID) as well as the Irish Research Council (No. EBPPG-2020-278).

1125

Depositing biological segmentation datasets FAIRly

Dr Elaine Ho[1], Dr Dimitris Ladakis[1], Dr Michele C. Darrow[1]
[1]Artificial Intelligence and Informatics, The Rosalind Franklin Institute, Harwell, United Kingdom

Poster Group 2

Background incl. aims
Segmentation of biological images identifies regions of an image which correspond to specific features of interest, which can be analysed quantitatively to answer biological questions. This task has long been a barrier to conducting large-scale biological imaging studies as it is time- and labour-intensive. Modern artificial intelligence segmentation tools can automate this process, but require high quality segmentation data for training, which is challenging to acquire. Biological segmentation data has been produced for many years, but this data is not often re-used to develop new tools as it is hard to find, access, and use. Recent disparate efforts [1-4] have been made to facilitate deposition and re-use of these valuable datasets, but more work is needed to increase re-usability. In this work, we review the current state of publicly available annotation and segmentation datasets and make specific recommendations to increase re-usability following FAIR (findable, accessible, interoperable, re-usable) principles [5] for the future.
Methods
A collection of publicly available segmentation and annotation datasets for 3-D volumetric electron microscopy and associated metadata was assembled from searches in the EMDB, EMPIAR, and Open Organelle databases, and a literature search with Pubmed from 2012-2023. Characteristics about these datasets were collected and trends over time were investigated, e.g., the purpose of the segmentations, data formats, biological feature type and size scale, imaging modality, and others.
Results
Whilst there were many examples of publicly available segmentation data that could be easily reused, these datasets were few and far between. We identified barriers to reusing published segmentation data according to FAIR principles. Many publications we reviewed were not findable or accessible as they were deposited at defunct URLs, were only available on request, or required researchers to search separately through citations or online to download the data. We found that data was deposited across at least 12 different formats, and 9 different online repositories, limiting the interoperability of these datasets as significant effort would be required to parse these formats into a single unified database for training segmentation tools. We found that there were considerable differences in the definitions of certain terms such as “segmentation”, “reconstruction”, and “ground truth”. A consensus is required across the breadth of the bioimaging community to ensure that these datasets can be re-used appropriately without misinterpretation.
Enhanced metadata capture and search capabilities would help developers find suitable datasets for their use case and determine how much (if any) manual curation would be required to bring segmentation data to the required standard for their study. This metadata could include the number and size of the feature being segmented relative to the image, the quality of the segmentation or the intended use of the dataset (qualitative visualisation, quantitative morphology, etc).
Conclusion
Re-use of biological segmentation data is important for enhancing development of segmentation software tools, particularly those using artificial intelligence techniques requiring large amounts of training data. Enhanced metadata capture, quality evaluation, community consensus in ontology and standardisation in data formats is required for encouraging re-use of these precious segmentation datasets.

Keywords:

Segmentation; annotation; volume electron microscopy

Reference:

1. Iudin A, et al. (2023). “EMPIAR: the Electron Microscopy Public Image Archive.” Nucleic Acids Res., 51, D1503-D1511. https://doi.org/10.1093/nar/gkac1062
2. C. Shan Xu, et al. (2021) “An open-access volume electron microscopy atlas of whole cells and tissues.” Nature. https://doi.org/10.1038/s41586-021-03992-4.
3. J. T. Vogelstein, et al. (2018) “A Community-Developed Open-Source Computational Ecosystem for Big Neuro Data.” Nature Methods, (11)15:846–847. https://doi.org/10.1038/s41592-018-0181-1
4. Chan Zuckerberg Imaging Institute 2023, CryoET Data Portal, accessed 3rd Apr 2024. https://cryoetdataportal.czscience.com/browse-data/datasets
5. Wilkinson, M., et al. (2016) “The FAIR Guiding Principles for scientific data management and stewardship.” Sci Data 3, 160018. https://doi.org/10.1038/sdata.2016.18

1174

The Impact of Dietary Haemoglobin on Nymphal Stages of I.ricinus: The gut volume EM reconstruction

Mgr., M.sc. František Kitzberger[1,2], RNDr. Ph.D. Veronika Urbanová[1], RNDr. CSc. Petr Kopáček[1], RNDr. Ph.D. Daniel Sojka[1], Mgr. Ph.D. Jan Perner[1], RNDr. Ph.D. Marie Vancová[1]
[1]Institute of Parasitology, Biology Centre of the Czech Academy of Sciences, Ceske Budejovice, Czech Republic, [2]Faculty of Science, Department of Physics, University of South Bohemia, Ceske Budejovice, Czech Republic

Poster Group 1

The tick is a ubiquitous parasite whose life is highly dependent on the haemoglobin of its host. Tick ability to synthesize its own haem group has been lost in the course of its evolution. The haem group is an inevitable part of the tick's reproduction, as the haem group is deposited on the eggs. Previous studies have shown that the adult females can survive even without the haem group, but the requirement of the nymphs is still unknown.
We observed the morphology of the tick nymph gut through SBF-SEM (Serial Block Face Scanning Electron Microscopy), followed by a 3D reconstruction of its inner structures, including the granules, which were identified by a parallel immunolabelling study of host albumin and haemoglobin. The total volume of 0.003 mm3 was reconstructed using MIB/deepMIB[1, 2] and then visualised using AMIRA (Thermo Fisher Scientific).
The results of our work presented here show the distribution of haemoglobin and albumin in the midgut cells and, in addition, the distribution of lipid droplets, which occupy the majority of the cells at this feeding time.
All these components are important for the metamorphosis of the nymph and for the further life of the adult males and females.
[1] Microscopy Image Browser: A platform for segmentation and analysis of multidimensional datasets
I. Belevich, M. Joensuu, D. Kumar, H. Vihinen and E. Jokitalo
PLoS Biology 2016 Jan 4;14(1):e1002340. doi: 10.1371/journal.pbio.1002340
[2] DeepMIB: User-friendly and open-source software for training of deep learning network for biological image segmentation
I. Belevich and E. Jokitalo
PLoS Comput Biol. 2021 Mar 2;17(3):e1008374. doi: 10.1371/journal.pcbi.1008374

1230

Tracking the Ultrastructure of Life with Serial Block-face Scanning Electron Microscopy

Dr. Alexandra Elli[1], Dr. Nathalie Braun[2], Dr. Dieter Lauer[2]
[1]Carl Zeiss Microscopy GmbH, Jena, Germany, [2]Carl Zeiss Microscopy GmbH, Oberkochen, Germany

Poster Group 1

Background incl. aims
Life happens in 3D. To unlock the secrets of life we must consider and understand different aspects. Images acquired with an electron microscope reveal insights into the ultrastructure with highest resolution. Scanning electron microscopy (SEM) is a versatile method to obtain high-resolution information on the nanometer scale. While traditionally used for topography measurements, modern SEMs in biomedical research are utilized increasingly to obtain large volume data of biological samples. Single images are snapshots of a complex three-dimensional architecture reduced to a 2D image. The acquisition of volume data is necessary to understand this complex architecture. New developments in hardware and software as well as in electron optics enable an ever-larger range of applications in 3D. Different techniques like serial section tomography (Array Tomography), Serial block-face SEM (SBF-SEM) and focus ion beam SEM (FIB-SEM) allow us to understand these volumes. On this poster, we present the latest developments in Serial block-face imaging realized as ZEISS Volutome. ZEISS Volutome enables the acquisition of large volumes at nanometer resolution in an automated, unattended way. Regardless of which biological sample is to be analyzed - whether individual cells surrounded by pure, non-conductive resin or large, densely packed tissues such as brain - ZEISS Volutome is developed to image any type of resin-embedded biological sample.

Methods
Serial block-face SEM (SBF-SEM) was first developed and communicated by Denk et al. in 2004 [1]. In SBF-SEM, an ultramicrotome inside the SEM chamber can cut down to 25 nm thick sections from a resin-embedded sample block. The exposed sample surface is imaged with an electron beam, then new sections are cut away with a diamond knife, and the newly exposed block-face surface is imaged. This cutting and imaging process is repeated until the structure of interest is completely imaged. The acquired EM images are processed and digitally aligned into a 3D data set. Cell compartments can be easily identified and segmented from this z-stack. The segmented 3D data set can be visualized, investigated, and statistically analyzed.

Results
Serial block-face Imaging is the appropriate solution to image and follow neurons with long and thin protrusions, such as dendrites and axons. It is well suited to trace neurons within the large volumes necessary to capture the often-unpredictable paths of these cells. ZEISS Volutome enables acquisition of large mosaic images over all three dimensions at high resolution. This is supported by the stability of the ultramicrotome stage solution. Once the cutting and imaging parameters are set-up, the experiment runs automatically and autonomously. Sections as thin as 25 nm with pixel sizes as small as 3 nm can be cut to follow the dendrites and axons precisely over long distances (Figure 1A).
Going beyond image acquisition, ZEISS arivis, the software for image processing, segmentation, and visualization, facilitates the analysis of your ultrastructural 3D data set to elucidate the path of the individual neurons and the network of cell organelles (example shown in Figure 1B). High resolution image acquisition is crucial for the identification of different cellular components; this is possible with ZEISS Volutome (Figure 1C).

Conclusion

In recent years a range of technical hurdles have been overcome and have extended the applicability of SBF-SEM. Most notably, a technique called Focal Charge Compensation has been developed to enable imaging of charge-prone biological samples [2] as well as the new high-sensitivity Volume BSE detector for high quality imaging at low kV. Unattended sectioning and imaging make this technique a convenient way to acquire large, ultrastructural 3D data sets.

Figure Caption

A, Large volume acquisition is needed to understand the neuronal network and the structure of the brain as well as to capture the unpredictable paths of these cells. B, Data set was processed and visualized with ZEISS arivis, in blue: cell nuclei, in red: mitochondria. C, Images were acquired with 3 nm pixel size, revealing different organelles. Data was acquired with ZEISS Volutome on a GeminiSEM 460, pixel size: 6nm (A+B) or 3nm (C), cutting thickness: 25 nm, EHT: 1.2 - 1.4 kV, Ip: 90 pA, dwell time: 0.8 - 1.6 µs.
Sample Courtesy of Christel Genoud, Université de Lausanne, EMF, 1015 Lausanne, Switzerland

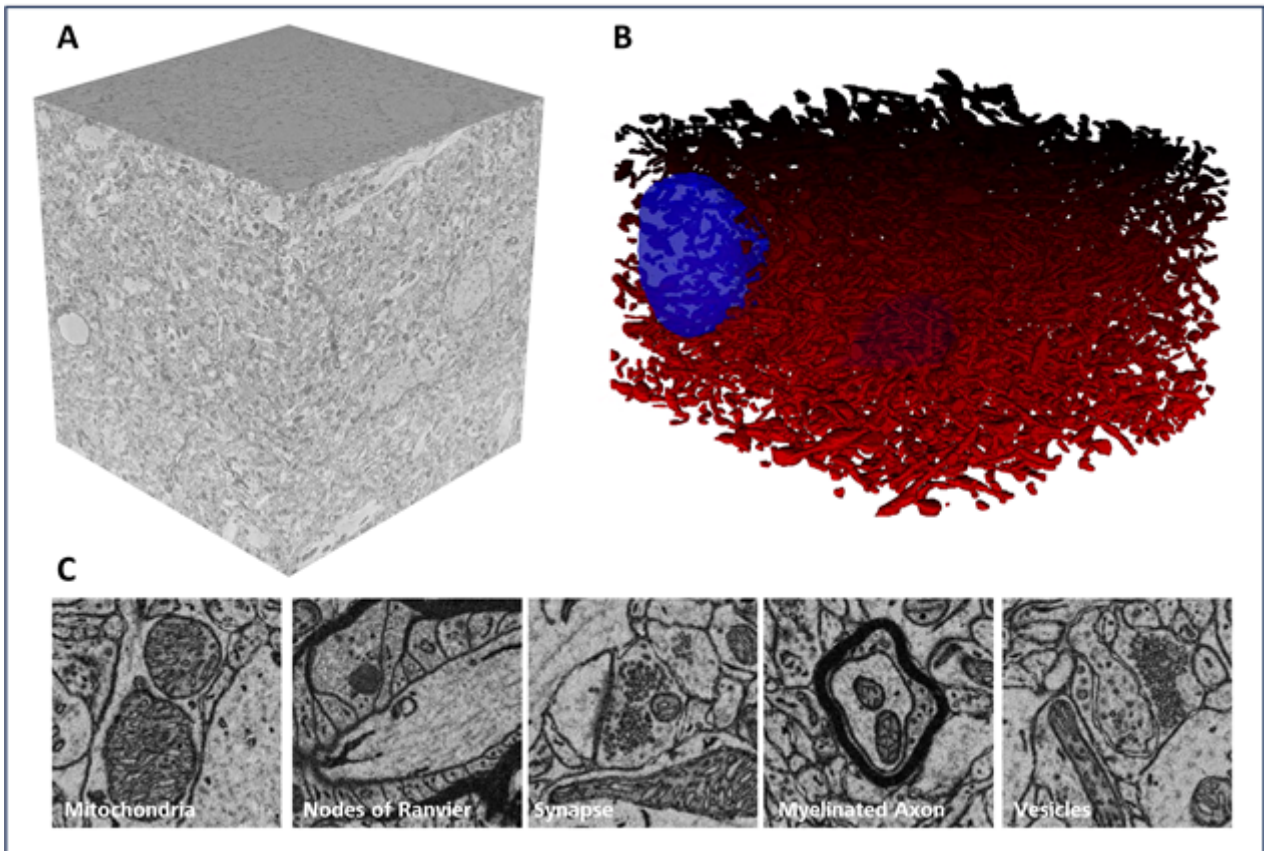

Keywords:

volumeEM, SBF-SEM, Cell biology, Neuroscience

Reference:

Reference:
[1] Denk W, Horstmann H (2004) Serial Block-Face Scanning Electron Microscopy to Reconstruct Three-Dimensional Tissue Nanostructure. PLoS Biol 2(11): e329.
[2] Deerinck TJ et al. (2018) High-performance serial block-face SEM of non-conductive biological samples enabled by focal gas injection-based charge compensation, J Microsc., 270(2): 142-149.

1239

3D imaging by Array Tomography using benchtop SEM

Kaori Nakajima[1], Yuuki Yamaguchi[1], Daisuke Masuda[1], Junichi Nakakobaru[2], Motohiro Nakamura[1], Katsuyuki Suzuki[1], Yukari Moriya[1], Yasuyuki Okano[1]
[1]JEOL Ltd., Akishima, JAPAN, [2]SYSTEM IN FRONTIER INC., Tachikawa, JAPAN

Poster Group 1

Background incl. aims
3D imaging is helpful for revealing the internal structure of biological tissues, microbes, and plants. This technique, especially for soft materials in micromorphology, has traditionally been performed using the tomography method with a transmission electron microscope (TEM). In recent years, scanning electron microscopes (SEM) have been used for 3D imaging by array tomography [1, 2], focused ion beam SEM (FIB-SEM), and serial block-face SEM (SBF-SEM). These SEM tomography methods are expected to be useful for many biological specimens because SEM can observe a wider region than TEM. Especially, the array tomography method is very useful due to the following features: fewer limitations on specimen size, the ability to re-observe sections, and the capability to perform correlative light electron microscopy (CLEM).
The array tomography method requires long acquisition times because it involves taking large number of photos over a wide area and through many sections. This method is generally performed using a high-resolution SEM, which is expensive and has a large footprint. Since benchtop SEMs are cheaper and have a smaller footprint, using multiple benchtop SEMs can be expected to increase throughput for large microstructures within a limited budget. Additionally, efficiency can be improved by first using 3D images obtained from benchtop SEMs to narrow down regions of interest. These selected regions can then be analyzed in detail with high-resolution SEMs.
The array tomography method using benchtop SEMs, which are manually operated to acquire images one by one, has been reported [3]. Modern benchtop SEMs, which have a motorized stage, can automatically perform array tomography similarly to high-resolution SEMs. In this report, we compare the 3D image quality between benchtop SEMs and high-resolution SEMs and discuss the possibility of the array tomography method using benchtop SEMs. Furthermore, we introduce the stage position linkage between both SEMs for the purpose of the efficient detailed analysis.

Methods
Paramecium was used as the model sample. Paramecium was cultured in water with gold, silver, and silica nanoparticles for 1 hour. The specimen was fixed with glutaraldehyde and OsO4 and then stained with uranyl acetate. The specimen was embedded in resin and sliced to a thickness of 200 nm. Three hundred sixty-six serial sections were placed on a carbon substrate (Ultra Flat Carbon: UFC, JEOL Ltd.). The serial sections were observed using a benchtop SEM (JCM-7000, JEOL Ltd.) and a high-resolution SEM (JSM-IT800<SHL>, JEOL Ltd.).

Results
3D reconstruction from the images of the serial sections was successful even with the benchtop SEM. The 3D reconstructed image obtained by the benchtop SEM is shown in Fig.1. In the cross-sectional image from the 3D reconstructed image, the paramecium (approximately 150 µm) and the phagosomes (approximately 10 µm) inside the paramecium were clearly recognized. However, in the benchtop SEM 3D image, the aggregation (approximately 1 µm) of nanoparticles in the phagosomes could not be clearly identified. This is because the spatial resolution of the benchtop SEM is poorer than that of the high-resolution SEM. Despite this, the benchtop SEM was able to perform array tomography and identify the macrostructure of the paramecium.

Conclusion

We succeeded in automatically capturing the images of the serial sections and demonstrated the effectiveness of array tomography on the benchtop SEM. The stage position linkage system between the benchtop SEM and the high-resolution SEM makes it possible to re-analyze the region of interest in detail and effectively.

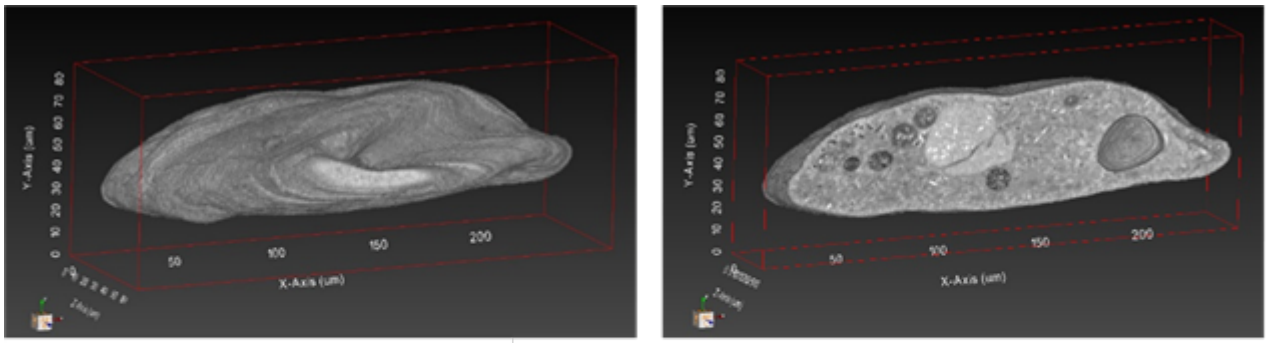

Figure 1. 3D reconstruction image of the paramecium obtained by benchtop SEM (left). One cross-sectional image from 3D reconstruction (right).

Keywords:

Array Tomography, Benchtop SEM

Reference:

1. Yamaguchi Y et al., Annual Meeting of The Japanese Society of Microscopy (2023).
2. Kubota Y. et al., Nature Commun. 9, 437 (2018).
3. Oi T., The 66th Symposium of the Japanese Society of Microscopy (2023).

1279

3D chromatin architecture by volume EM

Dr. Dusan Cmarko[1], Dr. Pavla Molinova[1], M.Sc. Marketa Dalecka[2], Dr. Ales Benda[3]
[1]Institute of Biology and Medical Genetics, First Faculty of Medicine, Charles University and General University Hospital in Prague, Prague, Czech Republic, [2]Imaging Methods Core Facility at BIOCEV and Department of Genetics and Microbiology, Faculty of Science, Charles University, Prague, Czech Republic, [3]Imaging Methods Core Facility at BIOCEV, Faculty of Science, Charles University, Prague, Czech Republic

Poster Group 1

Background
Detailed knowledge of the dynamic nuclear architecture is indispensable for understanding important nuclear functions such as DNA replication and repair, RNA synthesis, maturation, and transport. These processes occur in non-membrane chromatin-containing domains. Generally accepted opinion is that chromosomes reside in a certain area of the nucleus known as the chromosomal territories (CT). On the other hand, there is still disagreement over the interchromatin compartment, which is the DNA-free or DNA-poor nuclear region surrounding each individual CT. Our volume electron microscopy (EM) study set out to examine the distribution of DNA and chromatin inside the nuclear region, taking into account its extensive organization and functional role.

Methods
Light microscopy and fluorescent labels can provide an estimate of chromatin compaction and organization. For an understanding of the structural and functional organization of the cell nucleus in higher resolution, analysis of chromosomal domains at the ultrastructural level is essential.
To differentiate chromatin from other, especially, ribonucleoprotein containing structures, in EM, the cells were treated by pre-embedding staining where chromatin is observed as a highly contrasted structure. NAMA-Ur is method based on the extraction of RNA and phosphate groups from phosphoproteins by a weak alkali hydrolysis (NA) which does not affect DNA, followed by blockage of the amino and carboxyl groups by methylation and acetylation (MA). Finally, samples were stained by uranyl (Ur), which can bind to DNA, dehydrated and embedded in epoxy resin. Structural 3D acquisitions were performed using focused ion beam scanning electron microscopy (FIB-SEM). The obtained data was analysed by using Amira, NIS-Elements, and Imaris softwares. Nuclear subcompartments considered for analysis were as follows: perinuclear chromatin, perinucleolar chromatin, intranuclear chromatin, chromocenters, and interchromatin area.
Another analyses, which are currently in process, are comprised of function visualization of chromatin. To reveal the chromatin domains where gene transcription or replication take place, cells were labelled by in vivo incorporation of the nucleic acid precursors marked with halogens such as fluorine or bromine and/or by stable isotope 15N or 13C. Incorporated nucleotides were then observed either by combination of FIB-SEM with time-of-flight secondary ion mass spectrometry (SIMS) or by TEM with nanoscale SIMS (NanoSIMS). Moreover, serial sectioning of labeled cell nuclei is in progress for SEM followed by NanoSIMS as well as for array tomography.

Results
We successfully obtained a 3D datasets of NAMA-Ur-labeled nuclei by FIB-SEM acquisition with sufficient resolution and contrast for further quantification of perinuclear chromatin, perinucleolar chromatin, intranuclear chromatin, chromocenters, and interchromatin volumes.

Conclusion

The results demonstrate that the volume EM approaches performed on mammalian cell nuclei with specifically contrasted chromatin and eventually combining with spectrometry methods offer an extraordinary opportunity for study of nuclear architecture in situ and show great promise for novel achievements.

This work was supported by Charles University (Cooperatio). We acknowledge the Imaging Methods Core Facility at BIOCEV, institution supported by the Czech-Bioimaging large RI projects (LM2015062 and CZ.02.1.01/0.0/0.0/16_013/0001775, funded by MEYS CR) for support with obtaining data presented in this work.

Keywords:

Chromatin, Mammalian cells, Volume EM

Reference:

Testillano P.S. et al., J Histochem Cytochem. 1991;39(10):1427-38.
Rouquette J. et al., Chromosome Res. 2009;17(6):801-10.
Cremer T. et al., Bioessays. 2020;42(2):e1900132.